Ballistic spin transport in exciton gases

Alexey Kavokin, Maria Vladimirova, Benoit Jouault, Timothy Liew, Jason Leonard, Leonid Butov

Ballistic spin transport in exciton gases

A. V. Kavokin,[1,2] M. Vladimirova,[1] B. Jouault,[1] T. C. H. Liew,[3] J.R. Leonard,[4] and L.V. Butov[4]

[1] *Laboratoire Charles Coulomb, CNRS-Universite de Montpellier II, Pl. Eugene de Bataillon, 34095 Montpellier Cedex, France*

[2] *Physics and Astronomy School, University of Southampton, Highfield, Southampton, SO171BJ, UK*

[3] *Mediterranean Institute of Fundamental Physics, 31, via Appia Nuova, Roma, 00040, Italy*

[4] *Department of Physics, University of California at San Diego, La Jolla, CA 92093-0319, USA*

Traditional spintronics relies on spin transport by charge carriers, such as electrons in semiconductor crystals. The challenges for the realization of long-range electron spin transport include rapid spin relaxation due to electron scattering. Scattering and, in turn, spin relaxation can be effectively suppressed in excitonic devices where the spin currents are carried by electrically neutral bosonic quasi-particles: excitons or exciton-polaritons. They can form coherent quantum liquids that carry spins over macroscopic distances. The price to pay is a finite life-time of the bosonic spin carriers. We present the theory of exciton ballistic spin transport which may be applied to a range of systems supporting bosonic spin transport, in particular, to indirect excitons in coupled quantum wells. We describe the effect of spin-orbit interaction for the electron and the hole on the exciton spin, account for the Zeeman effect induced by external magnetic fields and long range and short range exchange splittings of the exciton resonances. We also consider exciton transport in the non-linear regime and discuss the definitions of the exciton spin current, polarization current and spin conductivity.

PACS numbers: 71.35.-y, 03.75.Kk, 03.75.Mn, 73.63.Hs, 78.55.Cr

I. INTRODUCTION

Excitons are electrically neutral and have finite life-times. These are two obstacles which make the development of excitonic spintronics, or spin-optronics challenging. How possibly one can explore the current, which is carried by neutral particles, and whose amplitude changes with distance and time? - is a fair question to ask. While electrons and holes have been considered as perfectly valid spin carriers, and exotic effects like the spin Hall effect[1] have been intensively studied for them[2–6], the spin currents carried by excitons[7–9] and exciton-polaritons[10,11] over tens or even hundreds of micrometers remained relatively less explored. There existed a huge imbalance of theoretical works on fermionic and bosonic spin transport. This is changing now. A number of phenomena have been observed and studied in the field of bosonic spin currents recently[7−26]. To summarize tens of publications in one sentence: bosonic systems bring new quantum coherent effects to the physics of spin transport. For instance, stimulation[23–25] and amplification[26] of spin currents are possible in exciton and exciton-polariton Bose gases. Bosonic spintronics or spin-optronics operates with electrically neutral spin carriers which makes control of spin currents carried by excitons a non-trivial task. Fortunately, the exciton density replaces charge in many aspects: the density currents may be efficiently controlled by stationary or dynamic potential gradients as demonstrated in recent works[27,28]. Combined with evident advantages of bosonic amplification and low dephasing, this makes spin-optronics a valuable alternative to fermionic spintronics. Besides bosonic effects, exciton spin transport has another important specific feature: it is dissipative by its nature, as the spin carriers have a finite (and short for excitons in regular materials) life-time. In continuous wave optical experiments stationary spin textures can appear: excitons are injected in the structure, they propagate ballistically or diffusively, and eventually disappear by radiative recombination. Their polarization properties and spin are inherited by the emitted photons, that is why the polarization patterns observed in near field photoluminescence experiments directly characterize exciton spin currents in the plane of the structure.

The goal of this work is to define what the exciton spin, magnetization and polarization currents are, and to explain how they can be described within the most frequently used spin density matrix (DM) approach and mean-field [29,30] approximation. We consider a specific system, namely a planar zinc-blend semiconductor structure containing quantum wells, where excitons can be formed. This choice is motivated by recent experimental results in GaAs/AlGaAs based coupled quantum wells. We limit the scope of this paper to heavy-hole excitons, however, our approach can be easily extended to light-hole excitons or excitons in quantum wells of a different symmetry. We do not speak here about the large variety of recent experimental results and application of the formalism presented here to the description of one particular experiment, as this would make this paper too long and too specific. For a direct comparison of theoretical simulations with the experimental data we address the reader to Ref. 8. The approaches formulated here are suitable for the description of a variety of excitonic spin effects in quantum wells.

The paper is organized as follows. In Section II we introduce the spin DM formalism accounting for the different mechanisms of spin re-orientation and the relation to electron and hole spin currents. In Section III we present numerical results obtained within the spin DM

formalism and analyze them. In Section IV we study the non-linear spin dynamics of propagating excitons using the Gross-Pitaevskii (GP) equations. The next three sections of the paper are devoted to exciton spin currents and polarization currents. Conclusions are perspectives are given in Section VIII.

II. THE SPIN MATRIX FORMALISM FOR PROPAGATING EXCITONS

In zinc-blend semiconductor quantum wells (e.g. in the most popular GaAs/AlGaAs system), the lowest energy exciton states are formed by electrons with spin projections on the structure axis of +1/2 and -1/2 and heavy holes whose quasi-spin (sum of spin and orbital momentum) projection to the structure axis is +3/2 or -3/2. Consequently, the exciton spin defined as the sum of the electron spin and heavy-hole quasi-spin may have one of four projections on the structure axis: +1,-1,+2,-2 [31]. These states are usually nearly degenerate, while there may be some splitting between them due to the short and long-range exchange interactions. Only the states with quasi-spin projections ±1 are coupled to the light, these are so-called bright states. The states with quasi-spin projections ±2 are called dark states.

It is important to note that the present formalism addresses the spin part of the exciton wavefunction, which is a product of electron and hole spin functions. For example, the probability to find the exciton in the spin state +1 is given by a product of probabilities to find an electron in the spin state -1/2 and the heavy hole in the spin state +3/2. The four component exciton wave-function is:

$$\begin{aligned}\Psi &= (\Psi_{+1}, \Psi_{-1}, \Psi_{+2}, \Psi_{-2}) \\ &= \Big(\Psi_{e,-\frac{1}{2}}\Psi_{h,+\frac{3}{2}}, \Psi_{e,+\frac{1}{2}}\Psi_{h,-\frac{3}{2}}, \\ &\qquad \Psi_{e,+\frac{1}{2}}\Psi_{h,+\frac{3}{2}}, \Psi_{e,-\frac{1}{2}}\Psi_{h,-\frac{3}{2}}\Big) \quad (1)\end{aligned}$$

where $\Psi_{e,+\frac{1}{2}}$ and $\Psi_{e,-\frac{1}{2}}$ are the components of the electron spinor wavefunction; $\Psi_{h,+\frac{3}{2}}$ and $\Psi_{h,-\frac{3}{2}}$ are the components of the heavy-hole spinor wavefunction.

To describe the dynamics of the system we will first define the Hamiltonian (Section II A) describing the different physical mechanisms of spin evolution. We then introduce the spin DM (Section II B) for the description of exciton spin states. We relate its components to the observable Stokes' vectors of light emitted by bright excitons and use the Liouville equation to describe its evolution in time. From the DM one can describe the polarization state of excitons and thus exciton spin currents. It is also instructive to consider the relationship with electron and hole spin currents (Section II C).

A. Hamiltonian

Here we derive the exciton Hamiltonian in the basis of +1,-1,+2,-2 states, accounting for the spin-orbit interaction (Dresselhaus and Rashba effects)[32,37], long- and short-range exchange interactions[33] and Zeeman effect, but neglecting exciton-exciton interactions, which will be discussed in the Section IV and neglecting magnetic field effect on center-of-mass motion and internal structure of exciton[34–36]. We consider excitons propagating ballistically in the plane of a quantum well. We shall characterize them by a fixed wave-vector, $\mathbf{k}_{\rm ex}$. We represent the full exciton Hamiltonian $\hat{\mathcal{H}}_{ex}^{tot}$ as a sum of three parts describing the spin-orbit and Zeeman effects on electrons, $\hat{\mathcal{H}}_{ex}^{e}$, and holes, $\hat{\mathcal{H}}_{ex}^{h}$, and the exchange induced splittings of exciton states, $\hat{\mathcal{H}}_{ex}^{ex}$:

$$\hat{\mathcal{H}}_{ex}^{tot} = \hat{\mathcal{H}}_{ex}^{e} + \hat{\mathcal{H}}_{ex}^{h} + \hat{\mathcal{H}}_{ex}^{ex}. \quad (2)$$

1. *Dresselhaus and Zeeman terms*

We recall that the Rashba-Dresselhaus effect is a momentum-dependent splitting of spin bands in two-dimensional semiconductor systems. It originates from a combined effect of the atomic spin orbit coupling and asymmetry of the potential in the direction perpendicular to the two-dimensional plane. This asymmetry comes either from the applied bias (which is described by the Rashba term in the Hamiltonian) or from the intrinsic asymmetry of the crystal lattice (described by the Dresselhaus term in the Hamiltonian). We shall separately consider both the Dresselhaus term (in this sub-section) and the Rashba term (in the next sub-section).

In order to build the 4×4 matrix Hamiltonian for excitons, we start with simpler 2×2 Hamiltonians describing the spin-orbit and Zeeman effects for electrons and holes.

The electron Hamiltonian in the basis of (+1/2,-1/2) spin states is:

$$\hat{\mathcal{H}}_e = \beta_e\left(k_{e,x}\hat{\sigma}_x - k_{e,y}\hat{\sigma}_y\right) - \frac{1}{2}g_e\mu_B\mathbf{B}\hat{\sigma}. \quad (3)$$

Here g_e is the electron g-factor, μ_B is the Bohr magneton, $\mathbf{B}$ is a magnetic field, $\hat{\sigma}$ is the Pauli matrix vector, and β_e is the Dresselhaus constant describing spin-orbit interactions of electrons. The Pauli matrix operators are:

$$\hat{\sigma}_z = \begin{bmatrix} 1 & 0 \\ 0 & -1 \end{bmatrix}, \quad \hat{\sigma}_y = \begin{bmatrix} 0 & -i \\ i & 0 \end{bmatrix}, \quad \hat{\sigma}_x = \begin{bmatrix} 0 & 1 \\ 1 & 0 \end{bmatrix}. \quad (4)$$

Rewriting Eq. (3) and retaining only z-component of the magnetic field, which corresponds to the Faraday geometry, one can obtain:

$$\begin{aligned}\hat{\mathcal{H}}_e &= \begin{bmatrix} -\frac{1}{2}g_e\mu_B B & \beta_e\left(k_{e,x}+ik_{e,y}\right) \\ \beta_e\left(k_{e,x}-ik_{e,y}\right) & \frac{1}{2}g_e\mu_B B \end{bmatrix} \\ &= \begin{bmatrix} -\frac{1}{2}g_e\mu_B B & \beta_e k_e e^{i\phi} \\ \beta_e k_e e^{-i\phi} & \frac{1}{2}g_e\mu_B B \end{bmatrix}, \quad (5)\end{aligned}$$

where ϕ is the angle between $\mathbf{k}_{\rm ex}$ and the chosen x-axis. The exciton Hamiltonian needs to be written in the basis of (+1,-1,+2,-2) exciton spin states, which correspond to (-1/2, +1/2, +1/2, -1/2) electron spin states. The electron spin-flip couples +1 and +2 states as well as -1 and -2 states. For each of these two couples of states we apply the Hamiltonian [Eq. (5)], which results in the following electronic contribution to the 4×4 exciton Hamiltonian:

$$\hat{\mathcal{H}}^{e}_{ex} = \begin{bmatrix} \frac{1}{2}g_e\mu_B B & 0 & \beta_e k_e e^{-i\phi} & 0 \\ 0 & -\frac{1}{2}g_e\mu_B B & 0 & \beta_e k_e e^{i\phi} \\ \beta_e k_e e^{i\phi} & 0 & -\frac{1}{2}g_e\mu_B B & 0 \\ 0 & \beta_e k_e e^{-i\phi} & 0 & \frac{1}{2}g_e\mu_B B \end{bmatrix} \tag{6}$$

2. Rashba terms

We note that another possible spin-orbit contribution to the Hamiltonian may come from the Rashba effect, which takes place in biased quantum wells. The Rashba term to be added in Eq. (3) is $\alpha_e\left(\hat{\sigma}_x k_{e,y} - \hat{\sigma}_y k_{e,x}\right)$, where α_e is a constant proportional to the Rashba field. The contribution of the Rashba term to the electron Hamiltonian, in the basis of (+1/2,-1/2) electron spin states, can be re-written:

$$\hat{\mathcal{H}}'_e = \begin{bmatrix} 0 & i\alpha_e k_e e^{-i\phi} \\ -i\alpha_e k_e e^{i\phi} & 0 \end{bmatrix}. \tag{7}$$

Using the same procedure as for Dresselhaus terms, this gives an additional contribution to the exciton Hamiltonian, in the basis of (-1/2, +1/2, +1/2, -1/2) electron spin states:

$$\hat{\mathcal{H}}^{e\prime}_{ex} = \begin{bmatrix} 0 & 0 & -i\alpha_e k_e e^{i\phi} & 0 \\ 0 & 0 & 0 & i\alpha_e k_e e^{-i\phi} \\ i\alpha_e k_e e^{-i\phi} & 0 & 0 & 0 \\ 0 & -i\alpha_e k_e e^{i\phi} & 0 & 0 \end{bmatrix} \tag{8}$$

Unless stated explicitly, we will for simplicity omit the Rashba terms in the rest of this paper and consider only the Dresselhaus terms. Note that there are no linear in wave-vector Rashba terms for heavy holes in zinc-blend quantum wells grown along the (001)-axis.

3. Heavy-hole contribution (Faraday geometry)

The heavy hole contribution to the Hamiltonian can be calculated with the reasoning similar to the electron case. The heavy-hole Hamiltonian written in the basis of (+3/2,-3/2) states is:

$$\hat{\mathcal{H}}_h = \beta_h\left(k_{h,x}\hat{\sigma}_x + k_{h,y}\hat{\sigma}_y\right) - \frac{1}{2}g_h\mu_B B\hat{\sigma}_z. \tag{9}$$

Here g_h is the heavy-hole g-factor and β_h is the Dresselhaus constant for heavy holes[32,37]. Note that the Dresselhaus Hamiltonian is different for heavy holes formed by p-orbital states and for conduction band electrons formed by s-orbital electronic states in a zinc-blend crystal lattice. The resulting from Dresselhaus coupling effective magnetic fields acting upon electron and heavy hole spins are oriented differently as well. Re-writing Eq. (9), we obtain:

$$\begin{aligned}\hat{\mathcal{H}}_h &= \begin{bmatrix} -\frac{1}{2}g_h\mu_B B & \beta_h\left(k_{h,x} - ik_{h,y}\right) \\ \beta_h\left(k_{h,x} + ik_{h,y}\right) & \frac{1}{2}g_h\mu_B B \end{bmatrix} \\ &= \begin{bmatrix} -\frac{1}{2}g_h\mu_B B & \beta_h k_h e^{-i\phi} \\ \beta_h k_h e^{i\phi} & \frac{1}{2}g_h\mu_B B \end{bmatrix}, \end{aligned} \tag{10}$$

The hole spin-flip couples +1 and -2 states as well as -1 and +2 states. For each of these two couples of states we apply the Hamiltonian (10), which results in the following hole contribution to the 4×4 exciton Hamiltonian:

$$\hat{\mathcal{H}}^{h}_{ex} = \begin{bmatrix} -\frac{1}{2}g_h\mu_B B & 0 & 0 & \beta_h k_h e^{-i\phi} \\ 0 & \frac{1}{2}g_h\mu_B B & \beta_h k_h e^{i\phi} & 0 \\ 0 & \beta_h k_h e^{-i\phi} & -\frac{1}{2}g_h\mu_B B & 0 \\ \beta_h k_h e^{i\phi} & 0 & 0 & \frac{1}{2}g_h\mu_B B \end{bmatrix} \tag{11}$$

4. In-plane magnetic field (Voight geometry)

If the magnetic field is applied in the plane, it splits electron and hole states polarized in the plane of the quantum wells. Suppose that the field is applied in the x-direction. In the electron and hole basis the Zeeman Hamiltonian is in this case:

$$\hat{\mathcal{H}}_{e,h} = -\frac{1}{2}g_{e,h}\mu_B B\hat{\sigma}_x = \begin{bmatrix} 0 & -\frac{1}{2}g_{e,h}\mu_B B \\ -\frac{1}{2}g_{e,h}\mu_B B & 0 \end{bmatrix}. \tag{12}$$

Note that the hole g-factor in plane of the quantum well is different from the g-factor in Faraday configuration, in general. This maps into the $(+1,-1,+2,-2)$ exciton basis as a Zeeman Hamiltonian of the form:

$$\hat{\mathcal{H}}_Z = -\frac{\mu_B B}{2}\begin{bmatrix} 0 & 0 & g_e & g_h \\ 0 & 0 & g_h & g_e \\ g_e & g_h & 0 & 0 \\ g_h & g_e & 0 & 0 \end{bmatrix} \tag{13}$$

5. Exchange terms

Besides the contributions from electron and hole spin orbit interactions and Zeeman splitting, there may be a purely excitonic contribution to the Hamiltonian, which is composed from the Hamiltonian for bright excitons written in the basis (+1,-1):

$$\hat{\mathcal{H}}_b = E_b\hat{I} - \delta_b\hat{\sigma}_x = \begin{bmatrix} E_b & -\delta_b \\ -\delta_b & E_b \end{bmatrix} \tag{14}$$

and the Hamiltonian for dark excitons written in the basis (+2,-2):

$$\hat{\mathcal{H}}_d = E_d\hat{I} - \delta_d\hat{\sigma}_x = \begin{bmatrix} E_d & -\delta_d \\ -\delta_d & E_d \end{bmatrix}, \tag{15}$$

where $\hat{I}$ is the identity matrix. The terms with δ_b and δ_d describe the splittings of bright and dark states polarized along x and y axes in the plane of the structure due to the long-range exchange interaction. The structural anisotropy is virtually inevitable even in the best quality epitaxially grown quantum wells. It arises from the reduced symmetry of heterointerfaces, from local strains and from islands of quantum well with fluctuations elongated in certain crystallographic directions. $E_b - E_d$ is the splitting between bright (+1 and -1) and dark (+2 and -2) exciton states due to the short-range exchange interaction. In microcavities, this splitting is additionally enhanced due to the vacuum field Rabi splitting of exciton-polariton modes formed by bright excitons and a confined optical mode of the cavity[38].

The origin of Eqs. (14) and (15) can be easily seen from the exciton Hamiltonian written in the basis of linear x and y polarizations. For example, for the bright excitons:

$$\hat{\mathcal{H}}_{XY} = \begin{bmatrix} E_b - \delta_b & 0 \\ 0 & E_b + \delta_b \end{bmatrix} \tag{16}$$

$$\hat{\mathcal{H}}_b = \hat{C}^{-1}\hat{\mathcal{H}}_{XY}\hat{C}, \tag{17}$$

where:

$$\hat{C} = \frac{1}{\sqrt{2}}\begin{bmatrix} 1 & 1 \\ i & -i \end{bmatrix}, \qquad \hat{C}^{-1} = \frac{1}{\sqrt{2}}\begin{bmatrix} 1 & -i \\ 1 & i \end{bmatrix} \tag{18}$$

are the transformation matrices from the linear to circular polarization basis and vice versa[39]. The same reasoning can be applied to the dark excitons as well.

The sum of Hamiltonians $\hat{\mathcal{H}}_b$ and $\hat{\mathcal{H}}_d$, written in the 4×4 exciton spin basis is:

$$\hat{\mathcal{H}}^{ex}_{ex} = \begin{bmatrix} E_b & -\delta_b & 0 & 0 \\ -\delta_b & E_b & 0 & 0 \\ 0 & 0 & E_d & -\delta_d \\ 0 & 0 & -\delta_d & E_d \end{bmatrix} \tag{19}$$

Now, the full exciton Hamiltonian can be written as:

$$\begin{aligned}\hat{\mathcal{H}}^{tot}_{ex} &= \hat{\mathcal{H}}^{e}_{ex} + \hat{\mathcal{H}}^{h}_{ex} + \hat{\mathcal{H}}^{ex}_{ex} \\ &= \begin{bmatrix} E_b + \frac{1}{2}(g_e - g_h)\mu_B B & -\delta_b & \beta_e k_e e^{-i\phi} & \beta_h k_h e^{-i\phi} \\ -\delta_b & E_b - \frac{1}{2}(g_e - g_h)\mu_B B & \beta_h k_h e^{i\phi} & \beta_e k_e e^{i\phi} \\ \beta_e k_e e^{i\phi} & \beta_h k_h e^{-i\phi} & E_d - \frac{1}{2}(g_e + g_h)\mu_B B & -\delta_d \\ \beta_h k_h e^{i\phi} & \beta_e k_e e^{-i\phi} & -\delta_d & E_d + \frac{1}{2}(g_e + g_h)\mu_B B \end{bmatrix}.\end{aligned} \tag{20}$$

For the translational motion of an exciton as a whole particle the exciton momentum is given by $\mathbf{P}_{ex} = (m_e + m_h)\,\mathbf{v}_{ex}$, where m_e and m_h are in-plane effective masses of an electron and of a heavy hole, respectively; $\mathbf{v}_{ex}$ is the exciton velocity. Having in mind that the exciton translational momentum is a sum of electron and hole translational momenta given by $\mathbf{P}_{\mathrm{e,h}} = m_{e,h}\mathbf{v}_{e,h}$, where $\mathbf{v}_e$ and $\mathbf{v}_h$ are the electron and hole velocity, respectively, one can easily see that $\mathbf{v}_h = \mathbf{v}_e = \mathbf{v}_{ex}$. Having in mind that $\mathbf{P}_{ex} = \hbar\mathbf{k}_{ex}$ and $\mathbf{P}_{e,h} = \hbar\mathbf{k}_{e,h}$, we have $\mathbf{k}_{ex} = \mathbf{k}_h + \mathbf{k}_e$, with $\mathbf{k}_e = \frac{m_e}{m_e+m_h}\mathbf{k}_{ex}$ and $\mathbf{k}_h = \frac{m_h}{m_e+m_h}\mathbf{k}_{ex}$. Thus, $\hat{\mathcal{H}}^{tot}_{ex}$ depends on the exciton center of mass wave-vector $\mathbf{k}_{ex}$ and on the angle ϕ between this angle and one of the structure axes (e.g. (100)-axis).

It should be noted that in this consideration the wavevectors $\mathbf{k}_{ex}, \mathbf{k}_h, \mathbf{k}_e$ are related to the translational motion of the exciton as a whole particle, with hole and electron as its constituents. The wave-vector of relative motion of the electron and hole "inside" the exciton is zero on average but may be important for each given moment of time. Recently, the effect of relative electron-hole motion on the spin-orbit effects of excitons has been analyzed by Vishnevsky *et al*[40] . Their analysis confirms the presence of linear in $\mathbf{k}_{ex}$ spin orbit terms in the exciton Hamiltonian introduced above.

B. Spin Density Matrix

Having constructed the Hamiltonian for excitons propagating with a wavevector $\mathbf{k}_{\mathrm{ex}}$, we now consider the description of their spin state. We shall use the spin density matrix, $\hat{\rho} = |\Psi\rangle\langle\Psi|$, where $\Psi = (\Psi_{+1}, \Psi_{-1}, \Psi_{+2}, \Psi_{-2})$ are the components of the exciton wavefunction projected onto the four spin states, $(|\Psi_{+1}\rangle, |\Psi_{-1}\rangle, |\Psi_{+2}\rangle, |\Psi_{-2}\rangle)$.

1. Relation to Stokes' vectors and polarization degrees of light

The exciton spin DM is given by:

$$\hat{\rho} = |\Psi\rangle\langle\Psi| = \begin{bmatrix} \Psi^*_{+1}\Psi_{+1} & \Psi^*_{-1}\Psi_{+1} & \Psi^*_{+2}\Psi_{+1} & \Psi^*_{-2}\Psi_{+1} \\ \Psi^*_{+1}\Psi_{-1} & \Psi^*_{-1}\Psi_{-1} & \Psi^*_{+2}\Psi_{-1} & \Psi^*_{-2}\Psi_{-1} \\ \Psi^*_{+1}\Psi_{+2} & \Psi^*_{-1}\Psi_{+2} & \Psi^*_{+2}\Psi_{+2} & \Psi^*_{-2}\Psi_{+2} \\ \Psi^*_{+1}\Psi_{-2} & \Psi^*_{-1}\Psi_{-2} & \Psi^*_{+2}\Psi_{-2} & \Psi^*_{-2}\Psi_{-2}, \end{bmatrix} \quad (21)$$

The elements of the upper left quarter of this DM are linked to the intensity of light emitted by bright exciton states, $I = \Psi^*_{+1}\Psi_{+1} + \Psi^*_{-1}\Psi_{-1}$, and to the components of the Stokes' vector, S_x, S_y and S_z of the emitted light:

$$\rho_{11} = \frac{I}{2} + S_z, \quad (22)$$

$$\rho_{12} = S_x - iS_y, \quad (23)$$

$$\rho_{21} = S_x + iS_y, \quad (24)$$

$$\rho_{22} = \frac{I}{2} - S_z. \quad (25)$$

These expressions can be summarized more succinctly using the Pauli matrices as:

$$\begin{bmatrix} \rho_{11} & \rho_{12} \\ \rho_{21} & \rho_{22} \end{bmatrix} = \frac{I}{2}\hat{I} + \mathbf{S}.\hat{\sigma}, \quad (26)$$

where $\mathbf{S} = (S_x, S_y, S_z)$ is the Stokes' vector and we recall that $\hat{I}$ is the identity matrix. Note that the trace of the spin density matrix is a number of particles in the system, which is not conserved because of the finite lifetime, in contrast with the full quantum optical density matrix which has the trace equal to unity.

Often when studying the polarization structure of fields with non-uniform intensity, it is useful to compare the polarization degrees of emitted light, which can be given by normalizing the Stokes' vectors to the light intensity. The circular polarization degree is:

$$\rho_c = \frac{2S_z}{I} = \frac{\rho_{11} - \rho_{22}}{\rho_{11} + \rho_{22}}. \quad (27)$$

The horizontal-vertical linear polarization degree is:

$$\rho_l = \frac{2S_x}{I} = \frac{\rho_{12} + \rho_{21}}{\rho_{11} + \rho_{22}}. \quad (28)$$

The linear polarization degree measured in the diagonal axes (also referred to as a diagonal polarization degree) is given by:

$$\rho_d = \frac{2S_y}{I} = i\frac{\rho_{12} - \rho_{21}}{\rho_{11} + \rho_{22}}. \quad (29)$$

2. Liouville equation

The dynamics of the DM is given by the quantum Liouville equation:

$$i\hbar\frac{d\hat{\rho}}{dt} = \left[\hat{\mathcal{H}}^{tot}_{ex}, \hat{\rho}\right], \quad (30)$$

where the Hamiltonian is composed from the electron, hole and exciton contributions given by Eqs. (6), (11) and (19) (considering the Faraday magnetic field configuration).

So far, we have neglected all relaxation or scattering processes in the system. The commonly used way to account for these processes is through the introduction of a phenomenological Lindblad superoperator to the Liouville equation:

$$i\hbar\frac{d\hat{\rho}}{dt} = \left[\hat{\mathcal{H}}^{tot}_{ex}, \hat{\rho}\right] - \hat{L}(\hat{\rho}), \quad (31)$$

where the Lindblad superoperator is introduced as:

$$\hat{L}(\hat{\rho}) = i\hbar \begin{bmatrix} \rho_{11}/\tau_b & \rho_{12}/\tau_b & \rho_{13}/\tau_c & \rho_{14}/\tau_c \\ \rho_{21}/\tau_b & \rho_{22}/\tau_b & \rho_{23}/\tau_c & \rho_{24}/\tau_c \\ \rho_{31}/\tau_c & \rho_{32}/\tau_c & \rho_{33}/\tau_d & \rho_{34}/\tau_d \\ \rho_{41}/\tau_c & \rho_{42}/\tau_c & \rho_{43}/\tau_d & \rho_{44}/\tau_d \end{bmatrix}. \quad (32)$$

τ_b is the bright exciton decoherence time, τ_d is the dark exciton decoherence time and τ_c is the characteristic decoherence time of processes between dark and bright excitons. Note that dissipation may be crucial in the description of exciton spin currents in realistic systems. In particular, within this formalism, in the presence of dissipation, the current conservation and flux conservation conditions become valid if completed by exciton generation and decay in the continuity equation. In the rest of this manuscript we shall neglect dissipation to simplify the model system and to clarify the physical mechanisms which govern the characteristics of exciton spin currents. Namely, we shall assume $\hat{L}(\hat{\rho}) = 0$. We stress that, in the experiment, the magnitude of predicted spin currents may be reduced by dissipation.

The formalism described so far, in sections II A and this section (II B), has been successfully applied in the description of spin transport in gases of cold excitons in coupled GaAs/AlGaAs quantum wells[8]. In this work, cold excitons are generated within localized spots and then fly away ballistically in radial directions. The elements of the DM, ρ_{ij}, are dependent on the distance from the excitation spot $\mathbf{r} = \mathbf{v}_{ex}t$ at time t and the polar angle, ϕ. The propagation speed $\mathbf{v}_{ex} = \hbar\mathbf{k}_{ex}/(m_e + m_h)$. In this work, when solving the Liouville equation introduced above, we shall refer to the experimental configuration of Ref. 8. In particular, this implies a specific choice of the initial conditions for Eq. (30): we shall assume that at zero time excitons are not moving. We shall assume that they populate the eigenstates of the exciton Hamiltonian $\hat{\mathcal{H}}^{tot}_{ex}$ taken with $\mathbf{k}_{ex} = 0$ following a thermal distribution with a temperature T. We shall assume that once created in the equilibrium state, the excitons start moving apart in the radial direction. Thus, implicitly, we account for a non-linear effect: dipole-dipole repulsion of excitons which makes them acquire a certain in-plane velocity $\mathbf{v}_{ex}$. This non-linearity is crucial to move the system out of equilibirum. The rest of exciton propagation and spin dynamics is modelled using the linear equation (30), where the Hamiltonian $\hat{\mathcal{H}}^{tot}_{ex}$ contains now the off-diagonal terms proportional to $\mathbf{k}_{ex}$.

C. Electron and hole spin currents

We shall normalize exciton, electron and heavy-hole functions to unity, namely:

$$\Psi^*_{+1}\Psi_{+1} + \Psi^*_{-1}\Psi_{-1} + \Psi^*_{+2}\Psi_{+2} + \Psi^*_{-2}\Psi_{-2} = 1 \quad (33)$$

$$\Psi^*_{e,+\frac{1}{2}}\Psi_{e,+\frac{1}{2}} + \Psi^*_{e,-\frac{1}{2}}\Psi_{e,-\frac{1}{2}} = 1 \quad (34)$$

$$\Psi^*_{h,+\frac{3}{2}}\Psi_{h,+\frac{3}{2}} + \Psi^*_{h,-\frac{3}{2}}\Psi_{h,-\frac{3}{2}} = 1 \quad (35)$$

Now, the exciton spin DM (21) can be represented in terms of electron and hole wavefunctions as:

$$\hat{\rho} = \begin{bmatrix} \Psi^*_{e,-\frac{1}{2}}\Psi_{e,-\frac{1}{2}}\Psi^*_{h,+\frac{3}{2}}\Psi_{h,+\frac{3}{2}} & \Psi^*_{e,+\frac{1}{2}}\Psi_{e,-\frac{1}{2}}\Psi^*_{h,-\frac{3}{2}}\Psi_{h,+\frac{3}{2}} & \Psi^*_{e,+\frac{1}{2}}\Psi_{e,-\frac{1}{2}}\Psi^*_{h,+\frac{3}{2}}\Psi_{h,+\frac{3}{2}} & \Psi^*_{e,-\frac{1}{2}}\Psi_{e,-\frac{1}{2}}\Psi^*_{h,-\frac{3}{2}}\Psi_{h,+\frac{3}{2}} \\ \Psi^*_{e,-\frac{1}{2}}\Psi_{e,+\frac{1}{2}}\Psi^*_{h,+\frac{3}{2}}\Psi_{h,-\frac{3}{2}} & \Psi^*_{e,+\frac{1}{2}}\Psi_{e,+\frac{1}{2}}\Psi^*_{h,-\frac{3}{2}}\Psi_{h,-\frac{3}{2}} & \Psi^*_{e,+\frac{1}{2}}\Psi_{e,+\frac{1}{2}}\Psi^*_{h,+\frac{3}{2}}\Psi_{h,-\frac{3}{2}} & \Psi^*_{e,-\frac{1}{2}}\Psi_{e,+\frac{1}{2}}\Psi^*_{h,-\frac{3}{2}}\Psi_{h,-\frac{3}{2}} \\ \Psi^*_{e,-\frac{1}{2}}\Psi_{e,+\frac{1}{2}}\Psi^*_{h,+\frac{3}{2}}\Psi_{h,+\frac{3}{2}} & \Psi^*_{e,+\frac{1}{2}}\Psi_{e,-\frac{1}{2}}\Psi^*_{h,-\frac{3}{2}}\Psi_{h,+\frac{3}{2}} & \Psi^*_{e,+\frac{1}{2}}\Psi_{e,+\frac{1}{2}}\Psi^*_{h,+\frac{3}{2}}\Psi_{h,+\frac{3}{2}} & \Psi^*_{e,-\frac{1}{2}}\Psi_{e,+\frac{1}{2}}\Psi^*_{h,-\frac{3}{2}}\Psi_{h,+\frac{3}{2}} \\ \Psi^*_{e,-\frac{1}{2}}\Psi_{e,-\frac{1}{2}}\Psi^*_{h,+\frac{3}{2}}\Psi_{h,-\frac{3}{2}} & \Psi^*_{e,+\frac{1}{2}}\Psi_{e,-\frac{1}{2}}\Psi^*_{h,-\frac{3}{2}}\Psi_{h,-\frac{3}{2}} & \Psi^*_{e,+\frac{1}{2}}\Psi_{e,-\frac{1}{2}}\Psi^*_{h,+\frac{3}{2}}\Psi_{h,-\frac{3}{2}} & \Psi^*_{e,-\frac{1}{2}}\Psi_{e,-\frac{1}{2}}\Psi^*_{h,-\frac{3}{2}}\Psi_{h,-\frac{3}{2}}, \end{bmatrix} \quad (36)$$

This representation allows us to obtain useful links between the elements of exciton, electron and hole density matrices, in particular:

$$\hat{\rho}_e = |\Psi_e\rangle\langle\Psi_e| = \begin{bmatrix} \Psi^*_{e,+\frac{1}{2}}\Psi_{e,+\frac{1}{2}} & \Psi^*_{e,-\frac{1}{2}}\Psi_{e,+\frac{1}{2}} \\ \Psi^*_{e,+\frac{1}{2}}\Psi_{e,-\frac{1}{2}} & \Psi^*_{e,-\frac{1}{2}}\Psi_{e,-\frac{1}{2}} \end{bmatrix} = \begin{bmatrix} \rho_{22}+\rho_{33} & \rho_{24}+\rho_{31} \\ \rho_{13}+\rho_{42} & \rho_{11}+\rho_{44} \end{bmatrix} \quad (37)$$

$$\hat{\rho}_h = |\Psi_h\rangle\langle\Psi_h| = \begin{bmatrix} \Psi^*_{h,+\frac{3}{2}}\Psi_{h,+\frac{3}{2}} & \Psi^*_{h,-\frac{3}{2}}\Psi_{h,+\frac{3}{2}} \\ \Psi^*_{h,+\frac{3}{2}}\Psi_{h,-\frac{3}{2}} & \Psi^*_{h,-\frac{3}{2}}\Psi_{h,-\frac{3}{2}} \end{bmatrix} = \begin{bmatrix} \rho_{11}+\rho_{33} & \rho_{14}+\rho_{32} \\ \rho_{23}+\rho_{41} & \rho_{22}+\rho_{44} \end{bmatrix} \quad (38)$$

We know that the components of electron and hole density matrices are linked with the projections of electron and hole spins as:

$$\hat{\rho}_e = \begin{bmatrix} \frac{1}{2}+S_{e,z} & S_{e,x}-iS_{e,y} \\ S_{e,x}+iS_{e,y} & \frac{1}{2}-S_{e,z} \end{bmatrix} \quad (39)$$

$$\hat{\rho}_h = \begin{bmatrix} \frac{1}{2}+S_{h,z} & S_{h,x}-iS_{h,y} \\ S_{h,x}+iS_{h,y} & \frac{1}{2}-S_{h,z} \end{bmatrix}, \quad (40)$$

where, for the heavy hole we have assigned spin +1/2 to the state +3/2 and spin -1/2 to the state -3/2 accounting for the orbital momentum of these states of +1 and -1, respectively.

The z-component of the spin polarization carried by electrons can now be expressed as:

$$S_{e,z} = (\rho_{22}+\rho_{33}-\rho_{11}-\rho_{44})/2. \quad (41)$$

Similarly, the z-component of the spin polarization carried by holes can now be expressed as:

$$S_{h,z} = (\rho_{11}+\rho_{33}-\rho_{22}-\rho_{44})/2. \quad (42)$$

The in-plane component of electron and hole spins can be extracted from the off-diagonal elements of the DM. Namely, the x-component of electron spin is given by:

$$S_{e,x} = (\rho_{13}+\rho_{31}+\rho_{24}+\rho_{42})/2, \quad (43)$$

while the x-component of the hole spin is given by:

$$S_{h,x} = (\rho_{14}+\rho_{23}+\rho_{32}+\rho_{41})/2. \quad (44)$$

The y-component of electron spin is given by:

$$S_{e,y} = i(-\rho_{13}+\rho_{31}+\rho_{24}-\rho_{42})/2, \quad (45)$$

while the y-component of the hole spin is given by:

$$S_{h,y} = i(\rho_{14}-\rho_{23}+\rho_{32}-\rho_{41})/2, \quad (46)$$

III. NUMERICAL RESULTS IN THE DENSITY MATRIX FORMALISM

Figure 1 shows the numerical results obtained within the DM formalism for a model system with the same parameters as those of coupled double quantum wells studied in Ref. 8. The parameters are summarized in Table I.

TABLE I: Parameters for numerical calculations.

Electron mass	m_e	0.07 m_0
Heavy hole mass	m_h	0.16 m_0
Electron Dresselhaus coupling	β_e	2.7 μeVμm
Heavy-hole Dresselhaus coupling	β_h	0.92 μeVμm
Bright exciton XY splitting	δ_b	0.5 μeV
Dark exciton XY splitting	δ_d	-13 μeV
Bright-dark exciton splitting	$E_b - E_d$	5 μeV

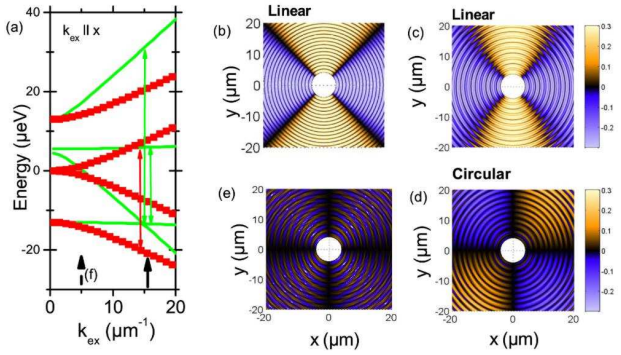

FIG. 1: (color online) (a) Dispersion of the excitonic states calculated using the set of parameters from Table I (green lines) and reduced set of parameters with $E_b - E_d = 0$, $\delta_b = 0$, $\beta_h = 0$ (red symbols). Black arrows indicate the values of the wavevectors used in (b)-(d) $k_{ex} = 15.3\mu\text{m}^{-1}$ and (e) $k_{ex} = 5\mu\text{m}^{-1}$. Double-ended arrows indicate the energies of oscillations between the eigenstates which appear in spatial polarization patterns. (b) Linear polarization degree along x-axis calculated with the simplified set of parameters. (c) Same as (b) but for the full set of parameters from the Table I. (d) Circular polarization degree with parameters from Table I. (e) Same but at $k_{ex} = 5\mu\text{m}^{-1}$. The source area was taken circular with a radius of 4μm.

The dispersion of bright and dark exciton modes obtained by diagonalisation of the Hamiltonian $\hat{\mathcal{H}}_{ex}^{tot}$ (20) is shown in Fig. 1(a) by green solid lines. The momentum has been chosen along the x direction, but the anisotropy of the band structure remains small. The initial splittings of dark and bright states makes these dispersion curves qualitatively different from those presented by Vishnevsky *et al*[40]. Note also, that Ref. ([40]) accounts for the exciton kinetic energy which we neglect in $\hat{\mathcal{H}}_{ex}^{tot}$, leaving only the spin-dependent contributions to the energy. The numerically calculated linear and circular polarization degrees are shown in Figs. 1(c) and (d), respectively. To stay close to the experimental conditions of Ref.[8], we have chosen as initial condition the circular source area with a radius of 4 μm, where cold excitons are generated within localized spots. In Fig.1(c), four lobes are unambiguously observable in the pattern of the linear and diagonal (not shown) polarizations. This pattern is a consequence of the Dresselhaus spin-orbit coupling for electrons, and it is characteristic of the chosen initial state at the source: four split eigen-states with zero in-plane wave-vector are occupied. Relative occupation of these states corresponds to the Boltzmann distribution at temperature $T = 0.1$ K. This choice of initial conditions leads to a variety of polarization patterns observed in experiment[8]. In the absence of the damping this pattern is periodic and infinite in the radial direction.

In order to reveal the mechanism of formation of the polarization patterns it is instructive to consider a simplified version of the Hamiltonian 20. In the absence of magnetic field, zero Dresselhaus effect for holes, zero splitting of bright excitons and zero splitting $E_b - E_d$ between bright and dark excitons this Hamiltonian can be rewritten as:

$$\hat{\mathcal{H}} = -\delta_d \begin{bmatrix} 0 & 0 & \xi e^{-i\phi} & 0 \\ 0 & 0 & 0 & \xi e^{i\phi} \\ \xi e^{i\phi} & 0 & 0 & 1 \\ 0 & \xi e^{-i\phi} & 1 & 0 \end{bmatrix} \tag{47}$$

where $\xi = -\beta_e k_e/\delta_d$. In other words, here we only take into account linear splitting of dark exciton states which inevitably results from structural anisotropy even in the best quality samples, and the Dresselhaus field acting on the spin of electron, bound to the hole. We will see that at sufficiently low temperature these two ingredients provide the in-plane asymmetry that ultimately results in the formation of linear polarisation patterns. Indeed, the eigenvalues of this Hamiltonian can be obtained analytically : $E = \pm\frac{1}{2}\delta_d \pm \frac{1}{2}\delta_d\sqrt{1+4\xi^2}$. This corresponds to two dispersion branches at low energy $\propto \pm\xi^2$ and two branches at high energy $\propto \pm(1+\xi^2)$ for $\xi \ll 1$. These branches are shown by red squares in Fig. 1(a).The eigenvectors, starting from the lowest energy and taking $\delta_d < 0$, can be approximated for small ξ by:

$$\begin{bmatrix} \xi e^{-i\phi} \\ -\xi e^{i\phi} \\ -1 \\ 1 \end{bmatrix}, \begin{bmatrix} e^{-i\phi} \\ e^{i\phi} \\ -\xi \\ -\xi \end{bmatrix}, \begin{bmatrix} e^{-i\phi} \\ -e^{i\phi} \\ \xi \\ -\xi \end{bmatrix}, \begin{bmatrix} \xi e^{-i\phi} \\ \xi e^{i\phi} \\ 1 \\ 1 \end{bmatrix}. \tag{48}$$

As mentioned already, at low temperatures $k_B T \ll |\delta_d|$, the lowest energy state with zero momentum is given by $[0, 0, -1, 1]$ and is a linearly polarized dark exciton. By linearly polarised dark exciton we mean the dark state which has a dipole moment oriented in a certain way, and which has a zero spin projection to the grows axis of the structure. After an acceleration due to dipole repulsion, this initial state is no longer an eigenstate and oscillates as a function of time between the two eigenstates of the Hamiltonian with which the initial state is not orthogonal, namely the first and the third eigenstates listed in Eqs. 48. Among these two states, only the third gives a significant contribution to the observed polarization as it is essentially "bright" (has large projections to $+1$ and -1 exciton states). The linear and diagonal polarizations originating from this state are readily given by $-\cos(2\phi)$ and $-\sin(2\phi)$ respectively. This reproduces the essential features of the numerical results for the linear polarization pattern, as one can see comparing the images calculated with the reduced Hamiltonian (Fig. 1(b)) and the full Hamiltonian (Fig. 1(c)). In the particular case considered here (initial state formed essentially by linearly polarized dark excitons) the Dresselhaus spin-orbit term for electrons leads to formation of the linear polarization vortex: the polarization plane is always perpendicular to the wave vector direction. The linear polarization vortex has been observed experimentally by High et al[8,9]. Rapid oscillations in radial direction are due periodical change in the occupation of mainly dark and

mainly bright states, indicated by double-ended arrows in Fig. (1(b)).

We should emphasize that with a proper reordering of the basis vectors, the simplified Hamiltonian 47 is analytically equivalent to the Hamiltonian of bilayer graphene. In its simplest expression, the Hamiltonian of bilayer graphene can be written as[41]:

$$\begin{bmatrix} 0 & v_F k e^{-i\phi} & 0 & 0 \\ v_F k e^{i\phi} & 0 & t_\perp & 0 \\ 0 & t_\perp & 0 & v_F k e^{-i\phi} \\ 0 & 0 & v_F k e^{i\phi} & 0 \end{bmatrix}. \quad (49)$$

where v_F is the velocity, k the amplitude of the momentum, ϕ the angle between the momentum and the x axis, and $t_\perp$ is the main coupling term between the two graphene layers, which is given by hopping between two carbon atoms that are superimposed. The four coefficients of the associated wavevectors correspond to the probability amplitudes on the two independent sublattices of the two graphene layers. By permutation of the basis vectors:$1 \to 1$, $2 \to 3$, $3 \to 4$, $4 \to 2$, the Hamiltonian is rewritten as:

$$\begin{bmatrix} 0 & 0 & v_F k e^{-i\phi} & 0 \\ 0 & 0 & 0 & v_F k e^{i\phi} \\ v_F k e^{i\phi} & 0 & 0 & t_\perp \\ 0 & v_F k e^{-i\phi} & t_\perp & 0 \end{bmatrix}. \quad (50)$$

which is equivalent to Eq. 47 with $t_\perp \equiv -\delta_d$ and $v_F k/t_\perp \equiv \xi$.

The 4×4 Hamiltonian of bilayer graphene is often restricted to the subspace of the two low energy bands. From Eq. 48, the corresponding eigenstates are:

$$[e^{i\phi}, \pm e^{-i\phi}]. \quad (51)$$

We can then define a pseudospin vector, which represents the relative phase between the two components of the wavevectors. From Eq. 51, the pseudospin rotates two times when the particle wavevector undergoes one full rotation.

Adapting the terminology used for graphene, the polarization pattern observed in Fig. 1(b,c) would be nothing else than the fingerprint of the "pseudospin" rotation in the exciton system. In the context of the exciton system under consideration, the phase ϕ corresponds to the angle between the exciton polarization vector and the chosen x-axis of the structure.

The build up of circular polarization requires introduction in the model of the splitting between linearly polarized bright exciton states δ_b . This splitting acts as an effective magnetic field applied to the Stokes vector of light emitted by bright excitons, $\mathbf{S} = (S_x, S_y, S_z)$. In particular, if the x-polarized exciton state has a lower energy than the y-polarized exciton state, it creates an effective magnetic field in the x-direction which rotates the Stokes vector in the yz plane. This converts the diagonal polarization to the circular polarization and leads to the appearance of right- and left-circularly polarized sectors in the polarization map of exciton emission. Separation of spins due to linear-to-circular polarization conversion is known in exciton-polariton systems as the *Optical spin Hall effect*. This effect was theoretically predicted in Ref. 12 and experimentally observed in polaritonic[10] and excitonic systems[8]. For microcavity polaritons it may be described in terms of beats between TE and TM polarized polariton modes, while in the exciton system studied here the effect is more complex due to the mixture of four nearly degenerate (dark and bright) exciton states. A recent theoretical paper[40] predicts the skyrmion formation in this case. Here we concentrate on the circular polarization patterns appearing due to the beats between linearly polarized exciton states mixed by the exchange interaction. Note that the circular polarization pattern is strongly sensitive to the chosen exciton wave-vector, which governs the energies of the four involved eigen-states. Figure 1(d) is calculated assuming $k_{ex} = 15.3\mu m^{-1}$. This corresponds to the crossing point of the dispersion branches associated to the first and second exciton eigen-states (see Fig 1(a)). For comparison, Fig. 1(e) shows the circular polarization pattern calculated with $k_{ex} = 5\mu m^{-1}$. One can see that the four lobes pattern of circular polarization is washed out, because the lowest energy state of the system remains essentially dark. Rapid oscillations that show up, have the period determined by the splitting between the two lowest states.

Finally, let us underline that the dispersion curves shown in Fig. 1(a) do not take into account the kinetic energy of excitons. The kinetic energy would shift all curves up by $K = \frac{\hbar^2 k_{ex}^2}{2m_{ex}}$. Note that this does not affect the splittings between exciton eigenstates and would not affect the spin dynamics of excitons. In the spin density formalism developed above we assign to all excitons the same kinetic energy, K. In a realistic system, the kinetic energy may be spread, in which case averaging of the obtained polarization patterns over k_{ex} may be needed. This averaging would smooth the fast oscillations seen on the images Fig. 1 (c,d,e,f). In the next section devoted to the non-linear spin dynamics we will fully take into account the kinetic energy of propagating excitons.

The distribution of in-plane projections of electron and hole spins for the same choice of parameters as above is shown in Figs. 2(a-h). The left panels show electron spins and the right panels show the hole spins. The direction of in-plane spin component is shown by arrows, while the length of each arrow is proportional to the computed value of the transverse spin component. The upper panels, Figs. 2(a,b), show the spin distributions in the absence of a magnetic field. In this case the electron and hole spins are oriented along the effective Dresselhaus fields which are oriented differently for electrons and heavy holes, as we have discussed in the previous section.

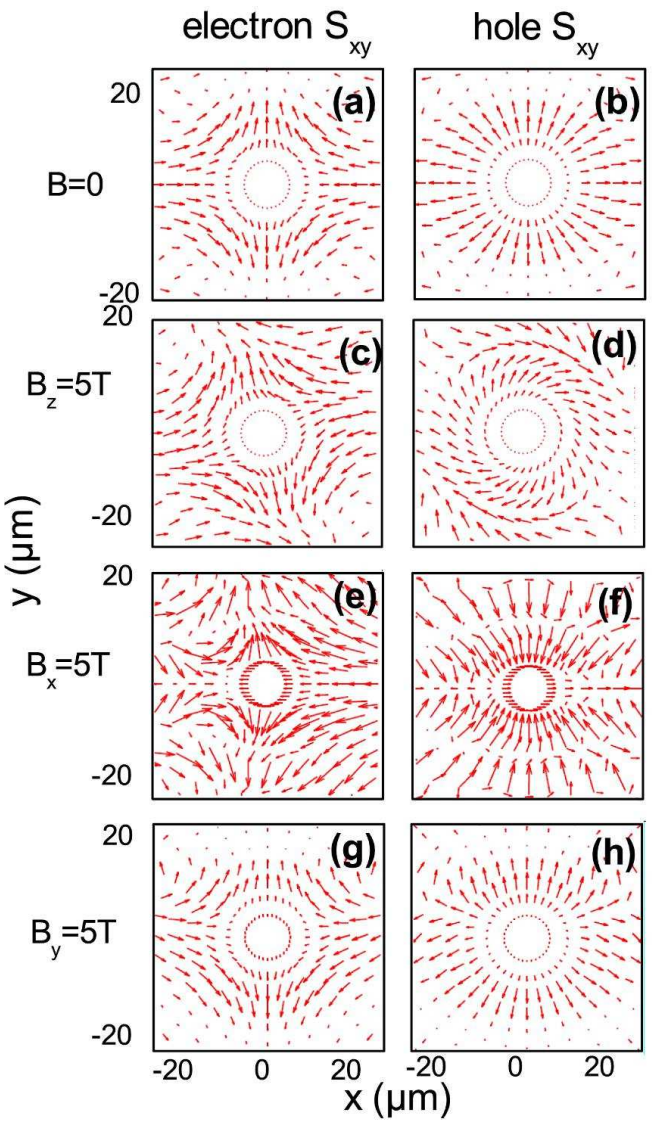

FIG. 2: (color online) Spatial distribution of electron and hole spin components in the plane of the quantum well structure, calculated at zero magnetic field and at $B = 5$ T at three different orientations. The parameters are given in Table I, at $\mathbf{k}_{ex} = 15.3\mu\text{m}^{-1}$ .The source area was taken circular with a radius of 4μm.

The decrease of the in-plane spin component upon propagation corresponds to the build-up of the z-component of electron and hole spins (Figure not shown), due to rotation of the exciton spin around the effective magnetic field. The magnetic field strongly changes the spin distribution in real space. The spin textures become strongly anisotropic in the case of in-plane (x- or y-oriented) magnetic field. Note, that the in-plane isotropy in the system is broken by the splitting between x- and y- polarized exciton states, which is why switching of the magnetic field between x and y axes strongly affects the distribution of electron and hole spins. It should be noted also that electron and hole in-plane spin textures can hardly be observed directly in optical experiments. However, they can be deduced from fitting the exciton polarization maps, e.g., using the formalism described above.

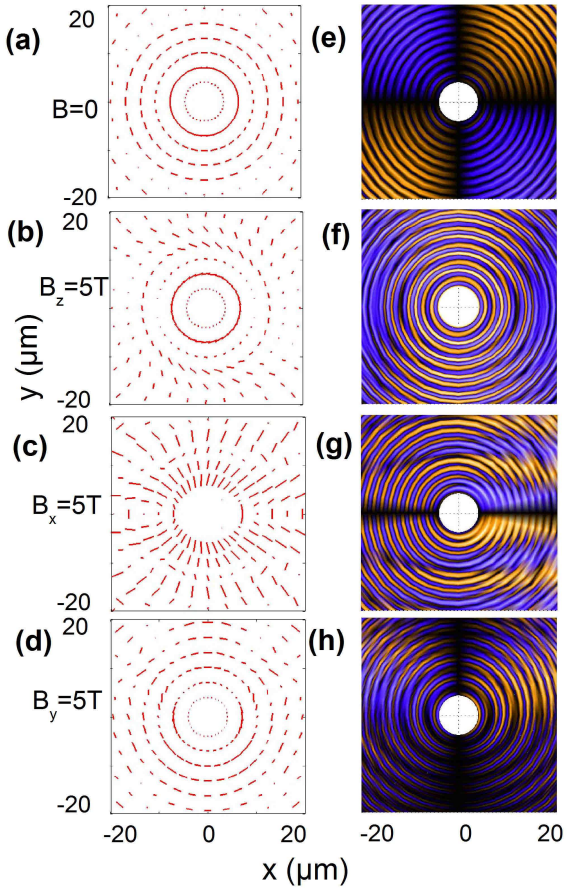

FIG. 3: (color online) Spatial distribution of exciton linear polarization ((a)-(d), length of the bars maps the intensity in arbitrary units) and color maps of the exciton circular polarization degree ((e)-(f)), same color code as in Fig. 1). Magnetic field $B = 0$ in (a), (e), and $B = 5$T along z in (b),(f), x in (c),(g), y in (d),(h). Parameters are given in Table I, $\mathbf{k}_{ex} = 15.3\mu\text{m}^{-1}$. The source area was taken circular with a radius of 4μm.

Figure 3 shows how the magnetic field affects spatial patterns of linear (a-d) and circular (e-h) polarization. Switching the magnetic field orientation between the x-, y- and z-axes one can dramatically affect the polarization patterns. Having in mind that the exciton polarization patterns can be directly observed in near-field photoluminescence experiments, fitting of these patterns to the experimental data would allow extracting the Dresselhaus constants and exciton exchange splittings, which, in turn, allow to restore electron and hole spin textures[8].

Figure 4(a-d) illustrates a peculiar regime where the Dresselhaus fields for electrons and holes are taken to be zero and there is no magnetic field applied, but electrons are subjected to the Rashba field (the Rashba field for heavy holes is zero). Figure 4(a) shows the electron spin distribution in space, where the spins are clearly aligned

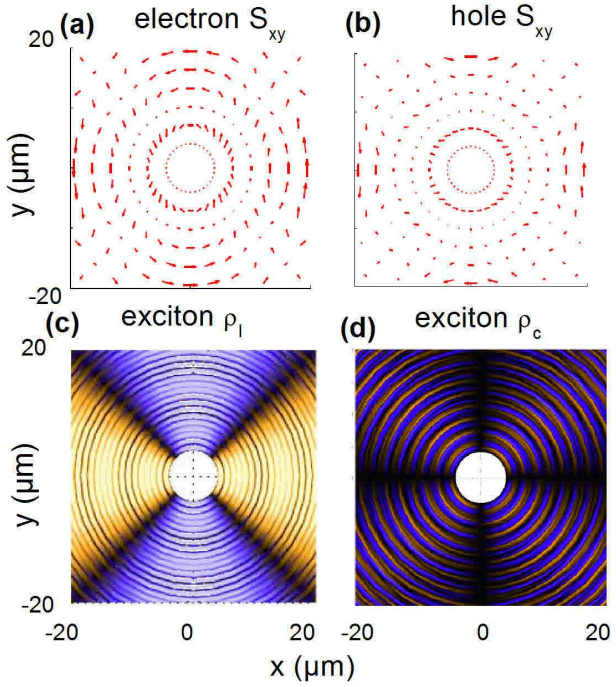

FIG. 4: (color online) Spatial distribution of electron (a) and hole (b) in-plane spin component calculated at B=0 in the absence of the Dresselhaus field $\beta_e = 0$; $\beta_h = 0$, but including Rashba field $\alpha_e = 2.7\mu$eVμm;. Other parameters are given in Table I, $\mathbf{k}_{ex} = 15.3\mu\text{m}^{-1}$. The source area was taken circular with a radius of 4μm. Corresponding patterns of linear (c) and circular (d) exciton polarization degree are shown with the same color code as in Fig. 1.

along the Rashba field force lines. Interestingly, the hole spins become polarized as well, while no effective field acts on them (Figure 4(b)). This is an illustration of the exciton effect: bound in excitons by Coulomb interaction and subject to the exchange induced exciton effects, the holes acquire in-plane spin polarization. The non-zero spin polarization of heavy holes is possible due to the exciton exchange effects. Figure 4(c,d) shows the resulting linear and circular exciton polarization patterns. One can see that the Rashba effect induces polarization patterns strongly different from those induced by the Dresselhaus effect, which is why from the shape of polarization patterns one can conclude on the nature of spin-orbit coupling in the system.

IV. NON-LINEAR SPIN DYNAMICS OF PROPAGATING EXCITONS AND EXCITON-POLARITONS

In the previous section we operated with a spin density matrix which is very convenient for the description of partially coherent and partially polarized exciton gases. The quantum Liouville equation (31) is a very efficient tool for the description of effects linear in the exciton density. On the other hand, one cannot straightforwardly incorporate non-linear interaction terms in this equation. The treatment of non-linear effects in a partially coherent system is a non-trivial task. Much simpler is the treatment of non-linear effects in a perfectly coherent system, such as a condensate at zero temperature. In this case, the ensemble of excitons can be described by a single 4-component wave function $\Psi = (\Psi_{+1}, \Psi_{-1}, \Psi_{+2}, \Psi_{-2})^T$. The linear dynamics of this wave-function for ballistically propagating excitons having a wavevector $\mathbf{k}_{ex}$ is described by the Schrödinger equation:

$$i\hbar \frac{d}{dt} |\Psi\rangle = \hat{\mathcal{H}} |\Psi\rangle , \tag{52}$$

where the Hamiltonian is the same as in Eq. (20). This equation represents a set of four coupled linear differential equations for four exciton spin components. Non-linear effects lead to the condensate evolution in real and reciprocal space.

From now on we shall consider the exciton spin dynamics in real space (2D), so that the wave function Ψ will become coordinate-dependent and will not be restricted to one single value of $\mathbf{k}_{ex}$. The non-linear interaction terms for multi-component exciton gases are introduced and discussed in detail in Ref. 42. Here we expand Eq. (52) by introducing the kinetic energy (to describe the real space dynamics) and the interaction terms. On the other hand, we neglect the magnetic field, for simplicity. This results in a system of four non-linear Schrödinger or GP equations[42–44]:

$$\begin{aligned} i\hbar\frac{d\Psi_{+1}}{dt} = &-\frac{\hbar^2\hat{\nabla}^2}{2m_{ex}}\Psi_{+1} + \frac{\beta_e m_e}{m_{ex}}\left(\hat{k}_x - i\hat{k}_y\right)\Psi_{+2} \\ &+ \frac{\beta_h m_h}{m_{ex}}\left(\hat{k}_x - i\hat{k}_y\right)\Psi_{-2} + \alpha_1 |\Psi_{+1}|^2 \Psi_{+1} \\ &+ \alpha_2 |\Psi_{-1}|^2 \Psi_{+1} + \alpha_3 |\Psi_{+2}|^2 \Psi_{+1} \\ &+ \alpha_4 |\Psi_{-2}|^2 \Psi_{+1} + W\Psi^*_{-1}\Psi_{+2}\Psi_{-2}, \end{aligned} \tag{53}$$

$$\begin{aligned} i\hbar\frac{d\Psi_{-1}}{dt} = &-\frac{\hbar^2\hat{\nabla}^2}{2m_{ex}}\Psi_{-1} + \frac{\beta_e m_e}{m_{ex}}\left(\hat{k}_x + i\hat{k}_y\right)\Psi_{-2} \\ &+ \frac{\beta_h m_h}{m_{ex}}\left(\hat{k}_x + i\hat{k}_y\right)\Psi_{+2} + \alpha_1 |\Psi_{-1}|^2 \Psi_{-1} \\ &+ \alpha_2 |\Psi_{+1}|^2 \Psi_{-1} + \alpha_3 |\Psi_{-2}|^2 \Psi_{-1} \\ &+ \alpha_4 |\Psi_{+2}|^2 \Psi_{-1} + W\Psi^*_{+1}\Psi_{+2}\Psi_{-2}, \end{aligned} \tag{54}$$

$$\begin{aligned} i\hbar\frac{d\Psi_{+2}}{dt} = &-\frac{\hbar^2\hat{\nabla}^2}{2m_{ex}}\Psi_{+2} + \frac{\beta_e m_e}{m_{ex}}\left(\hat{k}_x + i\hat{k}_y\right)\Psi_{+1} \\ &+ \frac{\beta_h m_h}{m_{ex}}\left(\hat{k}_x - i\hat{k}_y\right)\Psi_{-1} + \alpha_1 |\Psi_{+2}|^2 \Psi_{+2} \\ &+ \alpha_2 |\Psi_{-2}|^2 \Psi_{+2} + \alpha_3 |\Psi_{+1}|^2 \Psi_{+2} \\ &+ \alpha_4 |\Psi_{-1}|^2 \Psi_{+2} + W\Psi^*_{-2}\Psi_{+1}\Psi_{-1}, \end{aligned} \tag{55}$$

$$i\hbar\frac{d\Psi_{-2}}{dt} = -\frac{\hbar^2\hat{\nabla}^2}{2m_{ex}}\Psi_{-2} + \frac{\beta_e m_e}{m_{ex}}\left(\hat{k}_x - i\hat{k}_y\right)\Psi_{-1} + \frac{\beta_h m_h}{m_{ex}}\left(\hat{k}_x + i\hat{k}_y\right)\Psi_{+1} + \alpha_1\left|\Psi_{-2}\right|^2\Psi_{-2} + \alpha_2\left|\Psi_{+2}\right|^2\Psi_{-2} + \alpha_3\left|\Psi_{-1}\right|^2\Psi_{-2} + \alpha_4\left|\Psi_{+1}\right|^2\Psi_{-2} + W\Psi_{+2}^*\Psi_{+1}\Psi_{-1}. \quad (56)$$

Here $\hat{k}_{x,y} = -i\hat{\nabla}_{x,y}$, $m_{ex} = m_e + m_{hh}$. To make this system more compact we have omitted the terms describing exchange induced exciton splittings given by the Hamiltonian (20). We do not discuss here the nature and value of the interaction constants $\alpha_{1,2,3,4}$ and W. In the system of indirect excitons in coupled GaAs/AlGaAs quantum wells, as a zeroth approximation, one can take $\alpha_1 = \alpha_2 = \alpha_3 = \alpha_4$. Note also that in microcavities, where the lower exciton-polariton mode is strongly decoupled from dark excitons, the dark exciton states may be almost empty at low temperatures. If this is the case, the spin dynamics of the exciton-polariton condensate is given by the first two of the four GP equations (53 and 54) with $\alpha_{3,4} = W = 0$. The remaining constants $\alpha_{1,2}$ have been widely discussed in literature[45].

The GP equations are widely used for the description of coherent propagation of exciton-polaritons in microcavities[46]. They allow for the studying of interesting topology effects such as: quantum vortices[47–52]; half-quantum vortices[53–55]; bright[56] and dark[51,57–60] solitons.

The polarization of light emitted by an exciton or exciton-polariton condensate can be obtained as:

$$\rho_c = \frac{2S_z}{I} = \frac{\left|\Psi_{+1}\right|^2 - \left|\Psi_{-1}\right|^2}{\left|\Psi_{+1}\right|^2 + \left|\Psi_{-1}\right|^2}, \quad (57)$$

$$\rho_l = \frac{2S_x}{I} = \frac{2\mathcal{R}e\left\{\Psi_{+1}^*\Psi_{-1}\right\}}{\left|\Psi_{+1}\right|^2 + \left|\Psi_{-1}\right|^2}, \quad (58)$$

$$\rho_d = \frac{2S_x}{I} = -\frac{2\mathcal{I}m\left\{\Psi_{+1}^*\Psi_{-1}\right\}}{\left|\Psi_{+1}\right|^2 + \left|\Psi_{-1}\right|^2}. \quad (59)$$

These expressions easily follow from the definition of the spin density matrix.

A significant limitation of the GP equations as a theoretical tool is that they assume a coherent state of the system. If one is interested in the spin structure of the zero temperature ground state of excitons in a Bose-Einstein condensate[43], then this assumption is fulfilled by definition. However, in real systems there is an incomplete coherence that, strictly speaking, requires a description of statistical mixtures, perhaps involving density matrices. Furthermore, Eqs. (53-56) have been written assuming an infinite lifetime for the particles (be they excitons or exciton-polaritons), which is never the case of real non-equilibrium systems. Often pumping and radiative decay terms are introduced into Eqs. (53-56) phenomenologically[30,44]. While in the case of a resonant coherent pump, one can imagine that the exciton/exciton-polariton distribution inherits coherence directly, it is less obvious how an incoherent pump can be modelled. A phenomenological model introduced by Wouters and Carusotto[61] of incoherent pumping has allowed the modelling of the first order coherent fraction observed in many experimental configurations based on condensation[26,62–65]. While the GP model cannot model the phase transition during formation of a condensate and/or superfluid, it can offer a suitable description of spin currents once spatial coherence has formed.

Here we will consider a localized source of the four-component indirect exciton system, as corresponds to the localized bright spot sources generating exciton condensates[9]. We focus our attention on the possible spin polarization textures of coherent excitons propagating away from the source. We do not attempt to describe the partially coherent state within the source, noting that in exciton-polariton systems spin currents have been generated from both coherent[66] and incoherent[11] tightly focused spots utilizing the optical spin Hall effect[12] in a similar way. Since the Gross-Pitaevskii equations are only valid for coherent excitons, we restrict the exciton wavefunction to lie outside of the source area. The effect of the source is then characterized by the chosen boundary condition along the edge of the source area. Given that dark excitons have lower energy than bright excitons [due to the exchange splitting of Eq. (19)], it is reasonable to expect the source to provide linearly polarized dark excitons. By fixing the values of the exciton wavefunction along the edges of the source area, which is assumed circular, to such a distribution the boundary condition acts as an effective source for the exciton wavefunction outside the source area.

The indirect excitons are known to have very long lifetime, typically in the range of 10ns to 10μs[67]. This allows them to cover distances of a few hundreds of μm with negligible loss[8]. Consequently, when we focus on the behaviour of excitons in a small ($10 \times 10\mu m^2$) area around the source, the main loss of excitons is caused by their escape from the area of interest rather than their decay (recombination). To model the spin currents we thus employ an absorbing boundary condition to allow the solution of Eqs. (53-56) in a finite area. This allows a balance between source and loss to achieve a steady state of the non-equilibrium system (for a continuous pump), where both source and loss appear as boundary conditions.[8] The steady state solution of the system is independent of the initial condition.

Exciton intensity and polarization distributions calculated within the GP approach are shown in Figs. 5 and 7. Note that all the plotted quantities are spatially averaged over 1.5μm to account for the typical resolution of experimental setups[8]. In principle excitons can display features on the scale of the de Broglie wavelength, $\lambda = 2\pi/|\mathbf{k_{ex}}|$. Such features are on the sub-micron scale and are far beyond experimental resolution. We note also that while in the DM approach we could consider excitons having a fixed radial velocity, in the GP approach we necessarily cover the whole range of wavevectors and propagation velocities (the dispersion obtained from the

GP approach is shown in Fig. 6). Also, exciton-exciton interactions modify the exciton dispersion. For all these reasons, the DM and GP approaches cannot give identical results, in principle. The DM approach is suitable for the description of both coherent and partly coherent exciton gases, while the GP approach better catches the dispersive propagation features and accounts for nonlinear effects. Both approaches are complementary, and it is instructive to compare the results, obtained within these two models.

The exciton density decreases as excitons travel away from the source (Fig. 5a). This is not due to exciton recombination, which is expected to be very slow, but more simply due to the spreading out of excitons in all directions. The intensity spread need not be perfectly circularly symmetric due to the presence of the spin-orbit (Dresselhaus terms), which can introduce a directional dependence of the exciton velocity. Fig. 5b shows the exciton brightness degree, defined as:

$$\rho_b = \frac{|\Psi_{+1}|^2 + |\Psi_{-1}|^2 - |\Psi_{+2}|^2 - |\Psi_{-2}|^2}{|\Psi_{+1}|^2 + |\Psi_{-1}|^2 + |\Psi_{+2}|^2 + |\Psi_{-2}|^2}. \qquad (60)$$

This quantity represents the degree to which the bright exciton density exceeds the dark exciton density. There is a conversion of dark to bright excitons as they spread out from the source, which can be expected from the presence of Dresselhaus coupling terms.

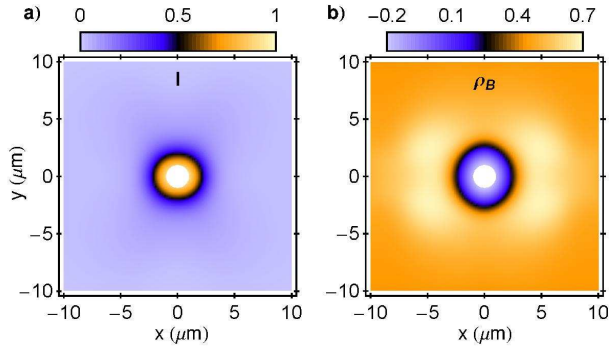

FIG. 5: (color online) Spatial distribution of the total exciton density (a) and exciton brightness degree (b) [see Eq. (60)] in the absence of a magnetic field. The parameters were the same as those used for the DM calculations, given in Table I, with: $B = 0$; $W = 0.2\alpha$; m_{ex} was taken as 0.21 of the free electron mass. The source area was taken circular with a radius of 1μm. The images are presented with spatial averaging over 1.5μm. The scattering parameter α and intensity at the source center were chosen such that the interaction energy, $\alpha\left(|\Psi_{+1}|^2 + |\Psi_{-1}|^2 + |\Psi_{+2}|^2 + |\Psi_{-2}|^2\right) = 1\mu$eV (being comparable to the other energy scales in the system, we are in a nonlinear regime). The absorbing boundary condition used in calculations appears outside of the plotted range, at a radius of 15μm from the source center.

The polarization distribution is shown in Fig. 7 and can be significantly influenced by non-linearity in the system. The left-hand plots show the results for negligible nonlinearity ($\alpha = 0$; $W = 0$), which is equivalent to a weak

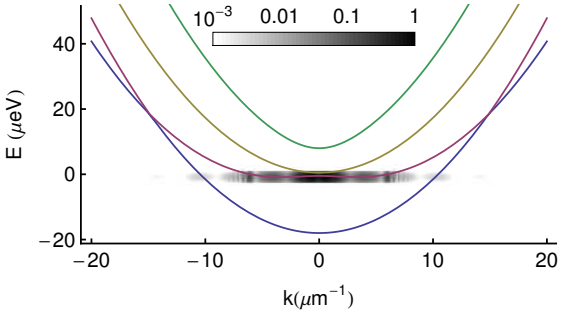

FIG. 6: (color online) Dispersion relation obtained from the Gross-Pitaevskii equations, corresponding to Figs. 5 and 7b,d and f. The dispersion is obtained by Fourier transform of the wavefunctions in space and time, from which the grayscale map of intensity is obtained. The curves show the bare dispersion, obtained from diagonalization of $\hat{\mathcal{H}}_{ex}^{tot} + \frac{\hbar^2 k^2}{2m}$.

pump intensity. Here the polarization distributions are qualitatively similar to those calculated in the density matrix formalism. In analogy to the (intrinsic) spin Hall effect[2,3] and the optical spin Hall effect[10,12] the presence of the spin-orbit coupling terms introduces a directional dependence of the polarization. The patterns of the polarization degrees divide into quadrants. Some quantitative differences with the DM calculations appear due to the presence of different wavevectors.

The right-hand plots show the case of a moderate nonlinearity, with interaction strength comparable to the other energy scales of the system. The most drastic effect is on the circular polarization degree, which becomes higher and each quadrant of circular polarization divides further giving an eight-lobed pattern to the polarization degree. The interaction terms that we have introduced are all spin conserving and it can be noted that we have considered the spin isotropic case. Even the W nonlinear interaction term, which allows the interconversion of bright and dark exciton pairs does not appear to directly change the spin polarization, conserving both circular and linear polarizations upon scattering. Still, the nonlinear interaction terms can have a drastic effect on the polarization structure. This is because they are able to shift (renormalize) the dispersion branches in the system. Given that the potential energy of excitons is fixed by their interaction energy at the source and that this energy is converted into kinetic energy at distances away from the source, any shifts in the dispersion branches can change the wavevector of propagating excitons. Even if the nonlinear induced shifts of the dispersion branches were not polarization dependent, a change in the wavevector of an exciton can allow it to experience a different effect from the k-dependent spin-orbit coupling terms. In this way, richer structures can appear in the nonlinear regime. Note, that the build-up of circular polarisation clearly seen in Fig. 7 (e,f) would not yield 100% circularly polarised excitons, as it might be expected in the ideal case of the optical spin Hall

effect for exciton-polaritons[12]. In our system, the precession of electron and hole spins has different frequencies, and the interplay between dark-to-bright and linear-to-circular polarisation conversion prevents formation of a purely circularly polarised state.

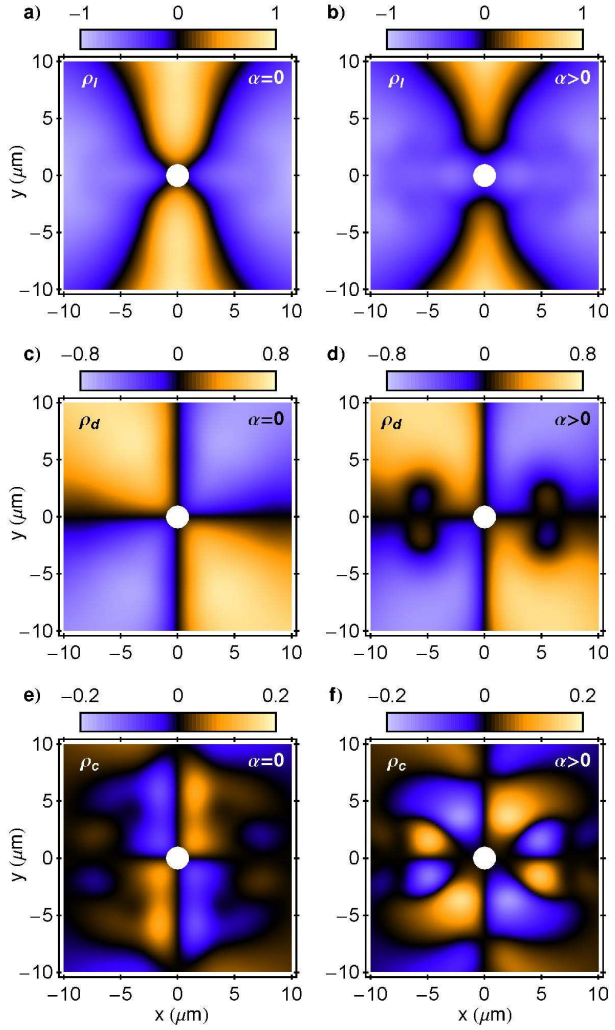

FIG. 7: (color online) Spatial distribution of the polarization state of excitons in the absence of a magnetic field: horizontal-linear polarization degree (a, b), diagonal polarization degree (c, d) and circular polarization degree (e, f) for bright excitons, which corresponds to the near field emission pattern of light. The left-hand plots show results in the absence of nonlinear interactions ($\alpha = 0$; $W = 0$), while the right-hand plots show the case of a moderate nonlinearity. The parameters were the same as in Fig. 5

V. EXCITON SPIN CURRENTS

Consider an exciton state characterized by a wavevector $\mathbf{k}_{ex}$ and described by the DM $\hat{\rho}$. Let us recall that the elements of this matrix ρ_{11}, ρ_{22}, ρ_{33}, ρ_{44} are the densities of +1,-1,+2 and -2 spin polarized excitons, respectively. The current of each of these densities is given by a product of the exciton speed and the corresponding density:

$$\mathbf{j}_a = \frac{\hbar \mathbf{k}_{ex}}{m_{ex}} \rho_{jj} \tag{61}$$

with $j = 1, 2, 3, 4$ for $a = +1, -1, +2, -2$, respectively. Experimentally, one can measure the magnetization current associated with the exciton density current. The magnetization carried by propagating excitons can be found as:

$$M_z = -\frac{\mu_B}{2\hbar} \left[(g_h - g_e)(\rho_{11} - \rho_{22}) + (g_h + g_e)(\rho_{33} - \rho_{44}) \right] \tag{62}$$

This expression is obtained having in mind that an electron with a spin projection on the z-axis of $\pm 1/2$ contributes to the magnetization projection on the z-axis $\mp \frac{\mu_B}{2} g_e$, and a heavy hole with the spin projection of $\pm 3/2$ contributes to the magnetization $\mp \frac{\mu_B}{2} g_h$. Hence, the magnetization (spin) current produced by the excitons having a wave-vector $\mathbf{k}_{ex}$ will be given by:

$$\mathbf{j}_M(\mathbf{k}_{ex}) = -\frac{\mu_B \mathbf{k}_{ex}}{2 m_{ex}} \left[(g_h - g_e)(\rho_{11}(\mathbf{k}_{ex}) - \rho_{22}(\mathbf{k}_{ex})) + (g_h + g_e)(\rho_{33}(\mathbf{k}_{ex}) - \rho_{44}(\mathbf{k}_{ex})) \right] \tag{63}$$

The total magnetization current in the exciton gas can be obtained by integration over all wave-vectors:

$$\mathbf{j}_M^{tot} = -\frac{A}{(2\pi)^2} \int \mathbf{j}_M(\mathbf{k}_{ex}) d\mathbf{k}_{ex} \tag{64}$$

Here A is the area of the sample. This current may be detected, for example, by spatially resolved Kerr rotation spectroscopy.

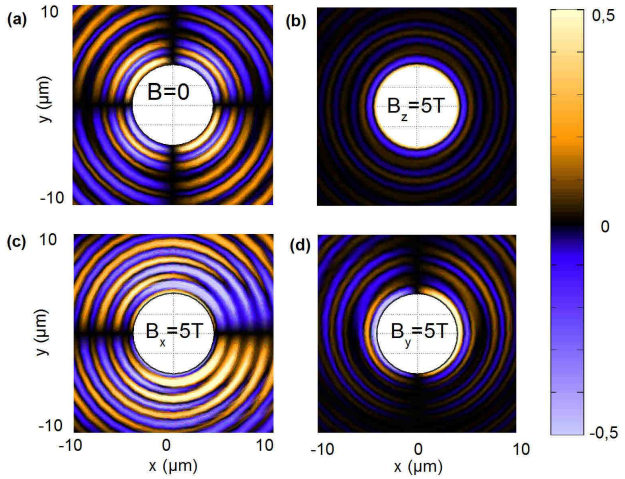

FIG. 8: (color online) Spatial distribution of the exciton spin current calculated in arbitrary units using the parameters summarized in Table I at $\mathbf{k}_{ex} = 15.3\mu\text{m}^{-1}$ at $B = 0$ (a) and $B = 5$T (b)-(d) along the z, x and y-axis, respectively. The source area was taken circular with a radius of 4μm.

Figure 8 shows the spin current density $\mathbf{j}_M / (2\pi r)$ calculated for the system of indirect excitons which we considered above in the absence of external magnetic field

(a) and in the presence of a magnetic field of 5T oriented normally to the plane of the structure (b) and along x- and y-axes (c,d). In all cases the current intensity decreases as one moves away from the excitation spot, as the exciton density decreases inversely with the radius r. One can see that the total spin (magnetization) of propagating excitons experiences oscillations and has a strong angular dependence. The spin currents are suppressed by an in-plane magnetic field, which is not surprising: $\mathbf{j}_M$ describes propagation of the normal-to plane spin component, which is strongly reduced by an in-plane magnetic field. The images show the total spin carried by both bright and dark excitons. They do not directly correspond to the polarized photoluminescence map for two reasons: first, dark excitons do not contribute to the photoluminescence; second, the polarization degree of photoluminescence does not experience the $1/r$ decay characteristic of the total spin density. On the other hand, the images presented in Figure 8 do correspond to the signal of spatially resolved Kerr or Faraday rotation, which is sensitive to the normal-to-plane magnetization.

VI. SPIN CURRENTS IN EXCITON CONDENSATES

The approach formulated above can be extended to the description of spin currents in coherent exciton (or exciton-polariton) condensates accounting for particle-particle interactions. In this case we need to replace the momentum $\hbar\mathbf{k}_{ex}$ by a momentum operator $\hat{p} = -i\hbar\hat{\nabla}$ and the diagonal components of the DM ρ_{11}, ρ_{22}, ρ_{33}, ρ_{44} by the exciton densities $|\psi_{+1}|^2, |\psi_{-1}|^2, |\psi_{+2}|^2, |\psi_{-2}|^2$, respectively, in the expressions 61 and 64. In this case the density currents become:

$$\mathbf{j}_\alpha = -i\frac{\hbar}{m_{ex}}\Psi_\alpha^*\nabla\Psi_\alpha, \tag{65}$$

and the total magnetization current can be expressed as:

$$\begin{aligned}\mathbf{j}_M^{tot} = \frac{i\mu_B}{2m_{ex}}\big[&(g_h - g_e)\left(\Psi_{+1}^*\nabla\Psi_{+1} - \Psi_{-1}^*\nabla\Psi_{-1}\right)\\ &+ (g_h + g_e)\left(\Psi_{+2}^*\nabla\Psi_{+2} - \Psi_{-2}^*\nabla\Psi_{-2}\right)\big]\end{aligned} \tag{66}$$

$$\begin{aligned}= -\frac{\mu_B}{2\hbar}\big[&(g_h - g_e)\left(\mathbf{j}_{+1} - \mathbf{j}_{-1}\right)\\ &+ (g_h + g_e)\left(\mathbf{j}_{+2} - \mathbf{j}_{-2}\right)\big]\end{aligned} \tag{67}$$

The distribution of the spin density current, $\mathbf{j}_{+1}$, is shown in Fig. 9 (a). The current density propagates outward from the source in all directions, decreasing in intensity. The apparent rotation of the current density is a nonlinear effect coming from the interactions in the system. The other spin density currents, $\mathbf{j}_{-1}$, $\mathbf{j}_{+2}$ and $\mathbf{j}_{+2}$, display a similar behaviour.

The magnetization current is shown in Fig. 9 (b). The current is stronger closer to the source, where the intensities are stronger. The magnetization current is predicted to rotate around the source.

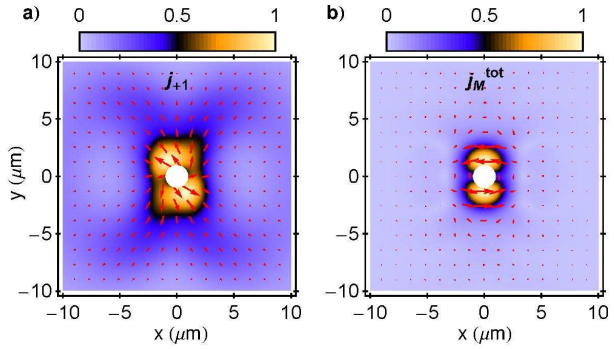

FIG. 9: (color online) Spatial structure of the spin density current $\mathbf{j}_{+1}$ (a) and the total magnetization current $\mathbf{j}_M^{tot}$ (b). The arrows show the directional dependence of the vector fields in space, while the colour code illustrates the intensity. The parameters were the same as in Fig. 5. Arbitrary units are used for both the spin density and total magnetization current.

One can also introduce the spin conductivity tensor linking the components of the density current (65) with the gradient of potential acting upon each of the exciton spin components:

$$j_{\alpha,l} = \sigma_{\alpha,\beta}^{l,m}\nabla U_{\beta,m}, \tag{68}$$

where $l = x, y$ and $m = x, y$ indicate the in-plane projections of the current and potential gradient, respectively. One can see that $\sigma_{\alpha,\beta}^{l,m}$ is a 64-component tensor in the general 2D case. The origin of the potential gradient $\nabla U_{\beta,m}$ needs to be discussed separately. $\nabla U_{\beta,m}$ can originate from the gradient of the quantum well width, gradient of the barrier height, or it can be induced by excitons themselves due to e.g. dipole-dipole repulsion. Indirect excitons have built-in dipole moments, the laterally modulated external electric field in the z-direction can create an in-plane potential landscape and, in turn,∇U for them. This was used in studies of transport of indirect excitons in various electrostatic potential landscapes including potential energy gradients[28,68,69], circuit devices[70–72], traps[73] lattices[74,75], moving lattices-conveyers[76], and narrow channels[72,77,78].

VII. POLARIZATION CURRENTS

Spatially resolved measurements of the polarization degrees ρ_c, ρ_l and ρ_d of light emitted by excitons give access to the exciton polarization currents. In terms of the DM formalism, they can be defined as products of the exciton

speed and the corresponding polarization degree:

$$\mathbf{j}_c\left(\mathbf{k}_{ex}\right)=\frac{\hbar\mathbf{k}_{ex}}{m_{ex}}\rho_c=\frac{\hbar\mathbf{k}_{ex}}{m_{ex}}\frac{\rho_{11}-\rho_{22}}{\rho_{11}+\rho_{22}} \tag{69}$$

$$\mathbf{j}_l\left(\mathbf{k}_{ex}\right)=\frac{\hbar\mathbf{k}_{ex}}{m_{ex}}\rho_l=\frac{\hbar\mathbf{k}_{ex}}{m_{ex}}\frac{\rho_{12}+\rho_{21}}{\rho_{11}+\rho_{22}} \tag{70}$$

$$\mathbf{j}_d\left(\mathbf{k}_{ex}\right)=\frac{\hbar\mathbf{k}_{ex}}{m_{ex}}\rho_d=\frac{\hbar\mathbf{k}_{ex}}{m_{ex}}\frac{\rho_{12}-\rho_{21}}{\rho_{11}+\rho_{22}} \tag{71}$$

The total polarization currents can be obtained integrating the expressions (69-71) over reciprocal space:

$$\mathbf{j}_{tot}^{c,l,d}=-\frac{A}{\left(2\pi\right)^2}\int d\mathbf{k}_{ex}\mathbf{j}_{c,l,d}\left(\mathbf{k}_{ex}\right) \tag{72}$$

The polarization currents in an exciton condensate can be found from the GP equations (53-56) as:

$$\mathbf{j}_c=-\frac{i\hbar}{m_{ex}}\frac{\left(\Psi_{+1}^*\nabla\Psi_{+1}-\Psi_{-1}^*\nabla\Psi_{-1}\right)}{|\Psi_{+1}|^2+|\Psi_{-1}|^2} \tag{73}$$

$$\mathbf{j}_l=-\frac{i\hbar}{m_{ex}}\frac{\left(\Psi_{+1}^*\nabla\Psi_{-1}+\Psi_{-1}^*\nabla\Psi_{+1}\right)}{|\Psi_{+1}|^2+|\Psi_{-1}|^2} \tag{74}$$

$$\mathbf{j}_d=-\frac{\hbar}{m_{ex}}\frac{\left(\Psi_{+1}^*\nabla\Psi_{-1}-\Psi_{-1}^*\nabla\Psi_{+1}\right)}{|\Psi_{+1}|^2+|\Psi_{-1}|^2} \tag{75}$$

The distributions of the polarization currents calculated within GP approach are shown in Fig. 10. A striking nonuniform structure appears due to the presence of the spin-orbit coupling terms. Close to the source spot, there is a strong circularly polarized current that rotates around the source. This can be attributed to the rotating circular polarization degree already observed in Fig. 7. Away from the source, the circular polarization current decays, which can be expected due to the decay of the spin density current observed in Fig. 9. Along the vertical axis ($x=0$), a strong circular polarization current remains due to the particularly fast change of the circular polarization degree in this region. The linearly polarized current can be stronger further away from the source than at closer distances. This is attributed to an increasing linear polarization degree further from the source. In addition, one can recall that while spin density currents are generally weaker further from the source, there is some compensation due to the conversion between dark and bright excitons (as shown in Fig. 5b, the bright exciton fraction increases further from the source).

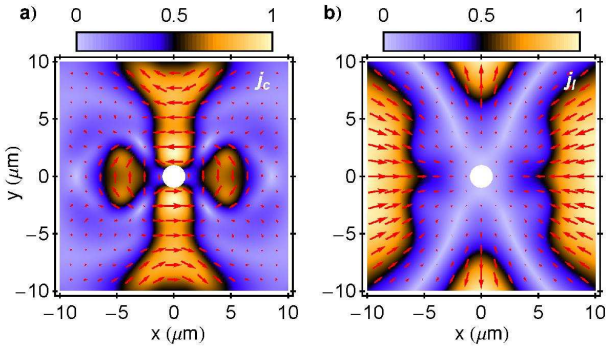

FIG. 10: (color online) Spatial structure of the polarization currents $\mathbf{j}_c$ (a) and $\mathbf{j}_l$ (b). The arrows show the directional dependence of the vector fields in space, while the colour code illustrates the intensity. The parameters were the same as in Fig. 5. Arbitrary units are used for the polarization currents.

VIII. CONCLUSIONS

Bosonic spin transport is a young and promising area of solid-state physics. The theories of mesoscopic transport of charge carriers and quantum transport are among the most interesting chapters of modern physics. Substitution of fermions by bosons and of a scalar electric charge by a spin vector cannot be formally done in these theories. Basically, all mesoscopic and quantum transport effects need to be reconsidered if we speak about electrically neutral bosonic spin carriers like excitons or exciton-polaritons. This is why the area of "spin-optronics" essentially remains *terra incognita*. Experimentally, direct measurements of transport of indirect excitons and exciton-polaritons in time-resolved imaging experiments have become possible in recent years. In this work, we have demonstrated that exciton polarization currents are inseparably connected with electron and hole spin currents. The intensity and direction of exciton polarization currents and electron and hole spin currents is governed by an interplay of spin-orbit effects, Zeeman effects and exciton exchange effects. In the non-linear regime, the pattern of spin currents may also be affected by spin-dependent exciton-exciton interactions.

We have developed two complementary approaches to the description of exciton spin currents and textures. The DM formalism allows for description of the spin transport effects in both classical exciton gases and condensates of non-interacting excitons, while the GP equations describe propagation of exciton condensates. We predict non-trivial topologies of interacting exciton spin in condensates, and suggest tools of their control, such as external magnetic and electric fields, and source intensity. We have demonstrated, that ballistic propagation of excitons may result in a build up of polarization patterns, which may be observed in near-field photoluminescence spectra.

This work has been supported by the EU FP7 ITN INDEX, EU FP7 PodiTrodi, the E.P.S.R.C., the EU FP7 Marie Curie EPOQUES, ANR-2011-NANO-004-06, and DOE. J. R. L. acknowledges Chateaubriand Fellowship from the Embassy of France in the United States. The authors are deeply grateful to T. Ostatnicky, Y.G. Rubo, M.M. Glazov, I.A. Shelykh, and A. Bramati for many useful discussions on the peculiarities of bosonic spin transport.

[1] M. I. Dyakonov and V. I. Perel, Phys. Lett. A, **35**, 459 (1971).
[2] J. Sinova, D. Culcer, Q. Niu, N. A. Sinitsyn, T. Jungwirth, and A. H. MacDonald, Phys. Rev. Lett., **92**, 126603 (2004).
[3] E. G. Mishchenko, A. V. Shytov and B. I. Halperin, Phys. Rev. Lett., **93**, 226602 (2004).
[4] Y. K. Kato, R. C. Myers, A. C. Gossard, and D. D. Awshalom, Science, **306**, 1910 (2004).
[5] J. Wunderlich, B. Kaestner, J. Sinova, and T. Jungwirth, Phys. Rev. Lett., **94**, 047204 (2005).
[6] S. O. Valenzuela and M. Tinkham, Nature **442**, 176 (2006).
[7] J. R. Leonard, Y. Y. Kuznetsova, Sen Yang, L. V. Butov, T. Ostatnicky, A. Kavokin, and A. C. Gossard, Nano Lett. **9**, 4294 (2009).
[8] A.A. High, A.T. Hammack, J.R. Leonard, Sen Yang, L.V. Butov, T. Ostatnicky, M. Vladimirova, A.V. Kavokin, T.C.H. Liew, K.L. Campman, A.C. Gossard, Phys. Rev. Lett., **110**, 246403, (2013).
[9] A. A. High, J. R. Leonard, A. T. Hammack, M. M. Fogler, L. V. Butov, A. V. Kavokin, K. L. Campman, and A. C. Gossard, **483**, 584, Nature, (2012).
[10] C. Leyder, T. C. H. Liew, A. V. Kavokin, I. A. Shelykh, M. Romanelli, J. Ph. Karr, E. Giacobino and A. Bramati, Nature Phys., **3**, 628 (2007).
[11] E. Kammann, T. C. H. Liew, H. Ohadi, P. Cilibrizzi, P. Tsotsis, Z. Hatzopoulos, P. G. Savvidis, A. V. Kavokin, and P. G. Lagoudakis, Phys. Rev. Lett., **109**, 036404 (2012).
[12] A. Kavokin, G. Malpuech, and M. Glazov, Phys. Rev. Lett., **95**, 136601 (2005).
[13] J. Keeling, Phys. Rev. B, **78**, 205316 (2008).
[14] J. Keeling, M. J. Bhaseen, and B. D. Simons, **105**, 043001 (2010).
[15] I. A. Shelykh, G. Pavlovic, D. D. Solnyshkov, and G. Malpuech, Phys. Rev. Lett., **102**, 046407 (2009).
[16] I. A. Shelykh, A. V. Kavokin, Y. G. Rubo, T. C. H. Liew, and G. Malpuech, Semicond. Sci. Technol., **25**, 013001 (2010).
[17] T. C. H. Liew, I. A. Shelykh, and G. Malpuech, Physica E, **43**, 1543 (2011).
[18] A. Amo, T. C. H. Liew, C. Adrados, R. Houdré, E. Giacobino, A. V. Kavokin, and A. Bramati, Nature Photon., **4**, 361 (2010).
[19] D. Sanvitto, S. Pigeon, A. Amo, D. Ballarini, M. De Giorgi, I. Carusotto, R. Hivet, F. Pisanello, V. G. Sala, P. S. S. Guimaraes, R. Houdré, E. Giacobino, C. Ciuti, A. Bramati, and G. Gigli, Nature Photon, **5**, 610 (2011).
[20] R. Hivet, H. Flayac, D. D. Solnyshkov, D. Tanese, T. Boulier, D. Andreoli, E. Giacobino, J. Bloch, A. Bramati, G. Malpuech, and A. Amo, Nature Phys., **8**, 724 (2012).
[21] J. Keeling and N. G. Berloff, Contempory Physics, **52**, 131 (2011).
[22] I. Carusotto and C. Ciuti, Rev. Mod. Phys. **85**, 299 (2013).
[23] M. H. Szymańska, F. M. Marchetti, and D. Sanvitto, Phys. Rev. Lett., **105**, 236402 (2010).
[24] A. Amo, D. Sanvitto, F. P. Laussy, D. Ballarini, E. del Valle, M. D. Martin, A. Lemaître, J. Bloch, D. N. Krizhanovskii, M. S. Skolnick, C Tejedor, L Viña, Nature, **457**, 291 (2009).
[25] C. Adrados, T. C. H. Liew, A. Amo, M. D. Martin, D. Sanvitto, C. Antón, E. Giacobino, A. Kavokin, A. Bramati, and L. Viña, Phys. Rev. Lett., **107**, 146402 (2011).
[26] E. Wertz, A. Amo, D. D. Solnyshkov, L. Ferrier, T. C. H. Liew, D. Sanvitto, P. Senellart, I. Sagnes, A. Lemaître, A. V. Kavokin, G. Malpuech, and J. Bloch, Phys. Rev. Lett., **109**, 216404 (2012).
[27] Y. Y. Kuznetsova, M. Remeika, A. A. High, A. T. Hammack, L. V. Butov, M. Hanson, and A. C. Gossard, Optics Letters, **35**, 1587 (2010).
[28] J.R. Leonard, M. Remeika, M.K. Chu, Y.Y. Kuznetsova, A.A. High, L.V. Butov, J. Wilkes, M. Hanson and A.C. Gossard, Appl. Phys. Lett. **100**, 231106 (2012).
[29] I. Carusotto and C. Ciuti, Phys. Rev. Lett., **93**, 166401 (2004).
[30] I. A. Shelykh, Y. G. Rubo, G. Malpuech, D. D. Solnyshkov, and A. Kavokin, Phys. Rev. Lett., **97**, 066402 (2006).
[31] See, e.g., E. L. Ivchenko and G. E. Pikus, "Superlattices and other heterostructures", *Symmetry and optical phenomena*, Springer, Berlin, (1997).
[32] E. I. Rashba and E. Ya. Sherman, Physics Letters A, **129**, 175 (1988).
[33] E. L. Ivchenko, "Optical spectroscopy of semiconductor nanostructures", *Alpha Science* (2005).
[34] L.P. Gor'kov, I.E. Dzyaloshinskii, Sov. Phys. JETP **26**, 449 (1968).
[35] I.V. Lerner, Yu.E. Lozovik, Sov. Phys. JETP **51**, 588 (1980).
[36] Yu.E. Lozovik, I.V. Ovchinnikov, S.Yu. Volkov, L.V. Butov, D.S. Chemla, Phys. Rev. B **65**, 235304, (2002).
[37] J.-W. Luo, A. N. Chantis, M. van Schilfgaarde, G. Bester, A. Zunger, Phys. Rev. Lett., **104**, 066405 (2010).
[38] See, e.g., A. V. Kavokin, J. J. Baumberg, G. Malpuech, and F.P. Laussy, "Microcavities", *Oxford University Press*, Oxford (2007).
[39] See, e.g., M. Born and E. Wolf, "Principles of optics", *Pergamon*, London, (1970).
[40] D. V. Vishnevsky, H. Flayac, A. V. Nalitov, D. D. Solnyshkov, N. A. Gippius, and G. Malpuech, Phys. Rev. Lett. **110**, 246404 (2013).
[41] E. McKann and M. Koshino, Reports on Progress in Physics, 056503 (2013).
[42] Y. G. Rubo and A. V. Kavokin, Phys. Rev. B, **84**, 045309 (2011).
[43] M. Matuszewski, T. C. H. Liew, Y. G. Rubo, and A. V. Kavokin, Phys. Rev. B, **86**, 115321 (2012)
[44] O. Kyriienko, E. B. Magnusson, and I. A. Shelykh, Phys. Rev. B, **86**, 115324 (2012).
[45] M. Vladimirova, S. Cronenberger, D. Scalbert, K. V. Kavokin, A. Miard, A. Lemaître, J. Bloch, D. Solnyshkov, G. Malpuech, and A. V. Kavokin, Phys. Rev. B, **82**, 075301 (2010).
[46] See, e.g., M. Wouters and I. Carusotto, Phys. Rev. Lett., **105**, 020602 (2010).
[47] D. M. Whittaker, Supperlattice. Microstruct., **41**, 297 (2007).
[48] T. C. H. Liew, A. V. Kavokin, and I. A. Shelykh, Phys. Rev. B, **75**, 241301 (2007).
[49] T. C. H. Liew, Yu. G. Rubo, and A. V. Kavokin, Phys. Rev. Lett., **101**, 187401 (2008).
[50] F. M. Marchetti, M. H. Szymanska, C. Tejedor, and D. M. Whittaker, Phys. Rev. Lett., **105**, 063902 (2010).
[51] S. Pigeon, I. Carusotto, and C. Ciuti, Phys. Rev. B, **83**,

144513 (2011).
[52] K. G. Lagoudakis, F. Manni, B. Pietka, M. Wouters, T. C. H. Liew, V. Savona, A. V. Kavokin, R. André, and B. Deveaud-Plédran, Phys. Rev. Lett., **106**, 115301 (2011).
[53] Yu. G. Rubo, Phys. Rev. Lett., **99**, 106401 (2007).
[54] H. Flayac, I. A. Shelykh, D. D. Solnyshkov, and G. Malpuech, Phys. Rev. B, **81**, 045318 (2010).
[55] F. Manni, K. G. Lagoudakis, T. C. H. Liew, R. André, V. Savona, and B. Deveaud-Plédran, Nature Communications, **3**, 1309 (2012).
[56] O. A. Egorov, D. V. Skryabin, and F. Lederer, Phys. Rev. B, **82**, 165326 (2010).
[57] A. V. Yulin, O. A. Egorov, F. Lederer, and D. V. Skryabin, Phys. Rev. A, **78**, 061801 (2008).
[58] H. Flayac, D. D. Solnyshkov, G. Malpuech, Phys. Rev. B, **84**, 125314 (2011).
[59] E. A. Ostrovskaya, J. Abdullaev, A. S. Desyatnikov, M. D. Fraser, and Y. S. Kivshar, Phys. Rev. A, **86**, 013636 (2012).
[60] A. Amo, S. Pigeon, D. Sanvitto, V. G. Sala, R. Hivet, I. Carusotto, F. Pisanello, G. Leménager, R. Houdré, E. Giacobino, C. Ciuti, and A. Bramati, Science, **332**, 1167 (2011).
[61] M. Wouters and I. Carusotto, Phys. Rev. Lett., **99**, 140402 (2007).
[62] G. Tosi, G. Christmann, N. G. Berloff, P. Tsotsis, T. Gao, Z. Hatzopoulos, P. G. Savvidis, and J. J. Baumberg, Nature Phys., **8**, 190 (2012).
[63] G. Christmann, G. Tosi, N. G. Berloff, P. Tsotsis, P. S. Eldridge, Z. Hatzopoulos, P. G. Savvidis, and J. J. Baumberg, Phys. Rev. B, **85**, 235303 (2012).
[64] V. Kohnle, Y. Léger, M. Wouters, M. Richard, M. T. Portella-Oberli, and B. Deveaud-Plédran, Phys. Rev. Lett., **106**, 255302 (2011).
[65] H. Flayac, G. Pavlovic, M. A. Kaliteevski, and I. A. Shelykh, Phys. Rev. B, **85**, 075312 (2012).
[66] A. Amo, T. C. H. Liew, C. Adrados, E. Giacobino, A. V. Kavokin, and A. Bramati, Phys. Rev. B, **80**, 165325 (2009).
[67] A.G. Winbow, A.T. Hammack, L.V. Butov, A.C. Gossard, Nano Lett. **7**, 1349 (2007).
[68] M. Hagn, A. Zrenner, G. Böhm, and G. Weimann, Appl. Phys. Lett. **67**, 232 (1995).
[69] A. Gärtner, A. W. Holleitner, J. P. Kotthaus, and D. Schuh, Appl. Phys. Lett. **89**, 052108 (2006).
[70] A. A. High, A. T. Hammack, L. V. Butov, M. Hanson, and A. C. Gossard, Opt. Lett. **32**, 2466 (2007).
[71] A. A. High, E. E. Novitskaya, L. V. Butov, M. Hanson, and A. C. Gossard, Science 321, 229 (2008).
[72] G Grosso, J Graves, A T Hammack, A A High, L V Butov, M Hanson, and A C Gossard, Nature Photon., **3**, 577 (2009).
[73] A. A. High, A. K. Thomas, G. Grosso, M. Remeika, A. T. Hammack, A.D. Meyertholen, M. M. Fogler, L. V. Butov, M. Hanson, and A. C. Gossard, Phys. Rev. Lett. **103**, 087403 (2009).
[74] M. Remeika, J. C. Graves, A. T. Hammack, A. D. Meyertholen, M. M. Fogler, L. V. Butov, M. Hanson, and A.C. Gossard, Phys. Rev. Lett. **102**, 186803 (2009).
[75] M. Remeika, M. M. Fogler, L. V. Butov, M. Hanson, and A. C. Gossard, Appl. Phys. Lett. **100**, 061103 (2012).
[76] A. G. Winbow, J. R. Leonard, M. Remeika, Y. Y. Kuznetsova, A. A. High, A. T. Hammack, L. V. Butov, J. Wilkes, A. A. Guenther, A. L. Ivanov, M. Hanson, and A. C. Gossard, Phys. Rev. Lett. **106**, 196806 (2011).
[77] X. P. Vögele, D. Schuh, W. Wegscheider, J. P. Kotthaus, and A. W. Holleitner, Phys. Rev. Lett. **103**, 126402 (2009).
[78] K. Cohen, R. Rapaport, and P. V. Santos, Phys. Rev. Lett. **106**, 126402 (2011).